

Stability, bifurcation, chaotic pattern, phase portrait and exact solutions of a class of semi-linear Schrödinger equations with Kudryashov's power law self-phase modulation and multiplicative white noise based on Stratonvich's calculus

Cheng-Qiang Wang(王成强), Xiang-Qing Zhao(赵向青), Yu-Lin Zhang(张玉林), and Zhi-Wei Lv(吕志伟)
Citation: Chin. Phys. B, 2025, 34 (**12**): 124205. DOI: 10.1088/1674-1056/ade664
http://cpb.iphy.ac.cn; http://iopscience.iop.org/cpb

What follows is a list of articles you may be interested in

Generation of mid-infrared supercontinuum by designing circular photonic crystal fiber

Ying Huang(黄颖), Hua Yang(杨华), and Yucheng Mao(毛雨澄)
Chin. Phys. B, 2022, 31 (**5**): 054211. DOI: 10.1088/1674-1056/ac272c

Variation of electron density in spectral broadening process in solid thin plates at 400 nm

Si-Yuan Xu(许思源), Yi-Tan Gao(高亦谈), Xiao-Xian Zhu(朱孝先), Kun Zhao(赵昆), Jiang-Feng Zhu(朱江峰), and Zhi-Yi Wei(魏志义)
Chin. Phys. B, 2021, 30 (**10**): 104205. DOI: 10.1088/1674-1056/abf0fe

Two-frequency amplification in a semiconductor tapered amplifier for cold atom experiments

Zhi-Xin Meng(孟至欣), Yu-Hang Li(李宇航), Yan-Ying Feng(冯焱颖)
Chin. Phys. B, 2018, 27 (**9**): 094201. DOI: 10.1088/1674-1056/27/9/094201

Generation of single and multiple dissipative soliton in an erbium-doped fiber laser

Li-Na Duan(段利娜), Jin Wen(文进), Wei Fan(樊伟), Wei Wang(王炜)
Chin. Phys. B, 2017, 26 (**10**): 104205. DOI: 10.1088/1674-1056/26/10/104205

Generation of few-cycle laser pulses: Comparison between atomic and molecular gases in a hollow-core fiber

Zhi-Yuan Huang(黄志远), Ye Dai(戴晔), Rui-Rui Zhao(赵睿睿), Ding Wang(王丁), Yu-Xin Leng(冷雨欣)
Chin. Phys. B, 2016, 25 (**7**): 074205. DOI: 10.1088/1674-1056/25/7/074205

Stability, bifurcation, chaotic pattern, phase portrait and exact solutions of a class of semi-linear Schrödinger equations with Kudryashov's power law self-phase modulation and multiplicative white noise based on Stratonvich's calculus

Cheng-Qiang Wang(王成强)[1,†], Xiang-Qing Zhao(赵向青)[1], Yu-Lin Zhang(张玉林)[2], and Zhi-Wei Lv(吕志伟)[1]

[1] *School of Mathematics and Physics, Suqian University, Suqian* 223800, *China*
[2] *School of Mathematics, Chengdu Normal University, Chengdu* 611130, *China*

(Received 13 March 2025; revised manuscript received 30 May 2025; accepted manuscript online 20 June 2025)

We devote ourselves to finding exact solutions (including perturbed soliton solutions) to a class of semi-linear Schrödinger equations incorporating Kudryashov's self-phase modulation subject to stochastic perturbations described by multiplicative white noise based on Stratonvich's calculus. By borrowing ideas of the sub-equation method and utilizing a series of changes of variables, we transform the problem of identifying exact solutions into the task of analyzing the dynamical behaviors of an auxiliary planar Hamiltonian dynamical system. We determine the equilibrium points of the introduced auxiliary Hamiltonian system and analyze their Lyapunov stability. Additionally, we conduct a brief bifurcation analysis and a preliminary chaos analysis of the auxiliary Hamiltonian system, assessing their impact on the Lyapunov stability. Based on the insights gained from investigating the dynamics of the introduced auxiliary Hamiltonian system, we discover 'all' of the exact solutions to the stochastic semi-linear Schrödinger equations under consideration. We obtain explicit formulas for exact solutions by examining the phase portrait of the introduced auxiliary Hamiltonian system. The obtained exact solutions include singular and periodic solutions, as well as perturbed bright and dark solitons. For each type of obtained exact solution, we pick one representative to plot its graph, so as to visually display our theoretical results. Compared with other methods for finding exact solutions to deterministic or stochastic partial differential equations, the dynamical system approach has the merit of yielding all possible exact solutions. The stochastic semi-linear Schrödinger equation under consideration can be used to portray the propagation of pulses in an optical fiber, so our study therefore lays the foundation for discovering new solitons optimized for optical communication and contributes to the improvement of optical technologies.

Keywords: stochastic semi-linear Schrödinger equations, self-phase modulation, soliton solutions, Stratonvich's calculus

PACS: 42.65.Tg, 42.65.Sf

DOI: 10.1088/1674-1056/ade664 **CSTR:** 32038.14.CPB.ade664

1. Introduction

Deterministic or stochastic nonlinear Schrödinger equations (NLSEs) describe a wide range of physical phenomena, including the well-known Bose–Einstein condensates and plasma physics.[1–4,6–10] For example, a model based on (deterministic) NLSEs was recently proposed by Kudryashov[2] to portray the soliton propagation in optical fibers. Exact solutions, including (perturbed) soliton solutions of deterministic or stochastic nonlinear partial differential equations (NLPDEs) not only offer insights into their solvability but also enhance our understanding of these equations' dynamical behaviors.[1,11–16] It was discovered in the literature that in (deterministic or stochastic) nonlinear dispersive wave PDEs (the Korteweg–de Vries equations, for instance), the delicate interplay between dispersion and nonlinearity enables the potential formation of traveling wave solutions, known as soliton solutions, which can retain their shape and energy over long distances. Thanks to this property, these types of PDEs, as with NLSEs, have extremely wide applicability in the real world.[17–20] As a consequence, various deterministic and stochastic NLPDEs have been extensively and intensively studied for their exact solutions, including (perturbed) soliton solutions, in recent years.[21–40,43–51] For example, Refs. [1,4–6,15,20,27,28,30–33,35–42] focused on NLSEs, while Refs. [19,24] investigated Fokas–Lenells equations. References [20,29] explored Schrödinger–Hirota equations, and Ref. [43] addressed the modified Korteweg–de Vries equation. References [17,21,45,46] examined Ginzburg–Landau equations, while Ref. [47] focused on the Biswas–Milovic equation. Reference [48] studied the Camassa–Holm equation, and Ref. [49] analyzed the Davey–Stewartson equation. Reference [50] investigated Gardner's equation, and Ref. [51] explored the Zakharov–Kuznetsov equation.

A model (based on deterministic NLSEs) proposed in Ref. [2] was shown to display self-phase modulation (SPM).

[†]Corresponding author. E-mail: chengqiangwang2022@foxmail.com

© 2025 Chinese Physical Society and IOP Publishing Ltd. All rights, including for text and data mining, AI training, and similar technologies, are reserved.

Inspired by results given in Ref. [2], Zayed *et al.*[25] studied stochastic NLSEs with Kudryashov's form of SPM having multiplicative white noise in terms of Itô's calculus. In Ref. [2], an algorithm based on the transformations for dependent and independent variables was utilized to find soliton solutions, and exact-soliton solutions in the form of kinks and optical solitons were given as the implicit functions. In Ref. [25], several soliton solutions were found via using a new mapping approach. Inspired by the interesting results reported in Refs. [2,25], we are concerned, in this paper, with a class of stochastic NLSEs with Kudryashov's form of SPM having multiplicative white noise based on Stratonvich's calculus. That is, we are focused on search for exact solutions (including perturbed soliton solutions) to the stochastic semi-linear Schrödinger equations (SSLSEs)

$$\begin{aligned}&\mathrm{i}\psi_t+\beta\psi_{xx}+(b_0|\psi|^{4\alpha}+c_0|\psi|^{3\alpha}+b_1|\psi|^{2\alpha}+c_1|\psi|^{\alpha}\\&+b_2)\psi+\mathrm{i}c_2\psi_x+c_3\psi_{xt}+\sigma(\psi-\mathrm{i}c_3\psi_x)\circ\frac{\mathrm{d}W(t)}{\mathrm{d}t}=0,\end{aligned}\quad(1)$$

in which the complex number $\mathrm{i}=\sqrt{-1}$ is the imaginary unit, the parameters α, β, σ, b_j and c_k are assumed to be real throughout this paper, $j=0,1,2$, $k=0,1,2,3$, the complex valued function $\psi=\psi(x,t)$ is the wave profile, $(x,t)\in\mathbb{R}^2$, $\beta\psi_{xx}$ is the chromatic dispersion (CD) term, $b_0|\psi|^{4\alpha}$, $c_0|\psi|^{3\alpha}$, $b_1|\psi|^{2\alpha}$ and $c_1|\psi|^{\alpha}$ are SPM terms, $\{W(t)\}_{t\in[0,+\infty)}$ is a given one-dimensional standard Brownian motion, the integration of the stochastic processes in this paper is understood in Stratonvich's sense. From now on, for any given function φ, we write formally φ_x (resp. φ_t) for the partial derivative of φ with respect to the space (resp. time) variable. Please refer to Refs. [2,25] for a more in-depth explanation of optical solitons having Kudryashov's self-phase modulation from the point of view of physics. The constant α, required to satisfy the condition $1<\alpha<2$, reflects the strength of the power-law nonlinearity of the SPM. The constant σ, required to obey the restriction $\sigma\neq 0$, is the intensity of the stochastic perturbations described by the Brownian motion $\{W(t)\}_{t\in[0,+\infty)}$.

As with Itô's calculus, Stratonovich's calculus is pervasive in theoretical research and applications.[52] It is well known that, in certain cases, Stratonovich's calculus is more applicable than Itô's calculus.[52,53] On the other hand, these two types of stochastic calculus formally obey the following rule:

$$\mathfrak{z}X(t)\circ\mathrm{d}W(t)=\mathfrak{z}X(t)\mathrm{d}W(t)+\frac{\mathfrak{z}^2}{2}X(t)\mathrm{d}t,$$

where $X(t)$ is a suitable stochastic process, $W(t)$ is, as above, a given one-dimensional standard Brownian motion, $\mathfrak{z}$ is a given complex number, $X(t)\mathrm{d}W(t)$ represents Itô's calculus, and $X(t)\circ\mathrm{d}W(t)$ represents Stratonovich's calculus. As far as the authors know, no research results have been reported in the literature on finding exact solutions to stochastic Schrödinger equations with Kudryashov's SPM structure having multiplicative white noise based on Stratonvich's calculus.

The main ingredient for studying exact solutions to the SSLSE in this paper is the dynamical system method. Our approach to this study can be described as follows. To obtain the desired exact solutions, we first apply a series of transformations of the dependent and independent variables to convert the concerned SSLSE into a second-order semi-linear ordinary differential equation (ODE), as in Refs. [2,25]. We then incorporate ideas from the sub-equation method to transform the resulting semi-linear ODE into an auxiliary planar Hamiltonian dynamical system. Next, we compute the equilibrium points of this Hamiltonian dynamical system and analyze their local Lyapunov stability, bifurcations, and chaotic behavior. Finally, we derive several exact solutions to the SSLSE under consideration by examining the dynamical properties of the auxiliary Hamiltonian system. Interested readers can refer to the extensive literature, such as Refs. [11,12,48], for more examples of applying the dynamical system method to find exact solutions to NLPDEs. In the literature, various other methods were devised to unveil exact solutions to (deterministic or stochastic) NLPDEs.[6,21,25,36,37,54–61] For example, Srivastava *et al.*[61] applied the modified Kudryashov method to the study of traveling wave solutions of nonlinear directional couplers, and Murad *et al.*[37] combined the Kudryashov method and Bernoulli's equation approach to study soliton solutions to higher-order NLSEs. Readers can also consult Ref. [55] for the tanh method, Ref. [56] for the modified extended tanh-function, Refs. [57,58] for the $\frac{G'}{G}$-expansion method, Ref. [60] for the $(\frac{G'}{G},\frac{1}{G})$-expansion method, Ref. [59] for the complete discrimination systems for polynomials method, Refs. [6,54] for the algebraic method, and Ref. [67] for the physics-informed neural network method. Compared to other methods for finding exact solutions to NLPDEs, the dynamical system method has the advantage of yielding all possible exact solutions.[11,12,48]

During the process of investigating the dynamical behaviors of the aforementioned Hamiltonian system, we identify all the equilibrium points which can help us find all possible exact solutions to the concerned SSLSE, as alluded previously. A bifurcation is a phenomenon in a nonlinear (ordinary or partial) differential equation where a slight variation in a parameter leads to a significant qualitative shift in the long-term behavior of the solution.[62–64] Chaos in a dynamical system refers to the phenomenon where small changes in the starting state lead to drastically different large-term behavior, making the system unpredictable despite being deterministic.[62,64,65] All the above dynamical system analyses help us gain a deeper understanding of the complexity of the exact solutions to the SSLSE (1) under consideration.

Apart from the introduction section, i.e., Section 1, which provides background information and objectives, the remainder of this paper is divided into five main sections, each covering a specific aspect of this study. In Section 2, we clearly formulate our problem, for SSLSE (1). In Section 3, we analyze in detail the dynamics of a planar Hamiltonian dynamical system associated with SSLSE (1). In Section 4, we provide several exact solutions to SSLSE (1) based on the results obtained in Section 3. In Section 5, we visualize some typical examples of the obtained soliton solutions to SSLSE (1) in Section 4. In Section 6, we offer several concluding remarks.

2. Statement of the concerned problem

In this section, we formulate the problem tackled in this paper through a sequence of variable changes. We are seeking exact solutions to SSLSE (1) in the form

$$\psi(x,t)=\Psi(x-vt)\,\mathrm{e}^{\mathrm{i}(\lambda x-(\omega+\sigma^2)t+\sigma W(t))}, \tag{2}$$

in which $\Psi=\Psi(\xi)$, $\xi\in\mathbb{R}$, denotes the amplitude of the profile function, the parameters λ, ω and v ($v\neq 0$) indicate the frequency, the wave number and the wave speed of the traveling solution $\Psi(x,t)$, respectively. Plugging Eq. (2) into the primal SSLSE (1), we obtain an auxiliary ODE involving Ψ as its unknown. Taking the imaginary part of the newly obtained auxiliary ODE, we obtain

$$\big(v-c_2-2\beta\lambda+c_3(\lambda v+\omega+\sigma^2)\big)\Psi'=0, \tag{3}$$

and taking the real part of the newly obtained auxiliary ODE, we arrive at

$$\begin{aligned}&(\beta-c_3v)\Psi''-\frac{c_3}{2}\sigma^2\Psi'+b_0\Psi^{4\alpha+1}\\&+c_0\Psi^{3\alpha+1}+b_1\Psi^{2\alpha+1}+c_1\Psi^{\alpha+1}\\&+\big(b_2+(1+\lambda c_3)(\omega+\sigma^2)-c_2\lambda-\beta\lambda^2\big)\Psi=0.\end{aligned} \tag{4}$$

To continue with our investigation, we impose the restrictions $c_3=0$ (resulting in the vanishing of the damping or anti-damping term $-\frac{c_3}{2}\sigma^2\Psi'$) and

$$v-c_2-2\beta\lambda+c_3(\lambda v+\omega+\sigma^2)=0, \tag{5}$$

or, equivalently, assume

$$\left.\begin{aligned}v&=c_2+2\beta\lambda,\\c_3&=0,\end{aligned}\right\} \tag{6}$$

to simplify Eqs. (3) and (4) into the following equation:

$$\begin{aligned}&\beta\Psi''+b_0\Psi^{4\alpha+1}+c_0\Psi^{3\alpha+1}+b_1\Psi^{2\alpha+1}+c_1\Psi^{\alpha+1}\\&+(b_2+\omega+\sigma^2-c_2\lambda-\beta\lambda^2)\Psi=0.\end{aligned} \tag{7}$$

As in Ref. [25], we put

$$\Psi(\xi)=\big(p(\xi)\big)^{\frac{1}{2\alpha}},\ \text{or equivalently,}\ p(\xi)=\big(\Psi(\xi)\big)^{2\alpha}, \tag{8}$$

where $p(\xi)$, required to be positive-valued, is yet to be determined. Plugging Eq. (8) into Eq. (7), we obtain

$$\begin{aligned}&2\alpha\beta pp''-\beta(2\alpha-1)p'^2+4b_0\alpha^2p^4\\&+4c_0\alpha^2p^{\frac{7}{2}}+4b_1\alpha^2p^3+4c_1\alpha^2p^{\frac{5}{2}}\\&+4\alpha^2(b_2+\omega+\sigma^2-c_2\lambda-\beta\lambda^2)p^2=0.\end{aligned} \tag{9}$$

Inspired again by Ref. [25], we also assume that

$$c_0=c_1=0. \tag{10}$$

Thus, we can simplify Eq. (9) to

$$\begin{aligned}&2\alpha\beta pp''-\beta(2\alpha-1)p'^2+4b_0\alpha^2p^4+4b_1\alpha^2p^3\\&+4\alpha^2(b_2+\omega+\sigma^2-c_2\lambda-\beta\lambda^2)p^2=0.\end{aligned} \tag{11}$$

Enlightened by the principle of homogeneity, we are tempted to assume now that a solution $p(\xi)$ to Eq. (11) automatically satisfies the following 'sub-equation':

$$p''=h_0p^3+h_1p^2+h_2p+h_3, \tag{12}$$

of which the first integral is

$$\frac{1}{2}p'^2=\frac{h_0}{4}p^4+\frac{h_1}{3}p^3+\frac{h_2}{2}p^2+h_3p+h_4. \tag{13}$$

Substituting Eqs. (12) and (13) into Eq. (11), and then rearranging the terms, we obtain

$$\begin{aligned}&3(8b_0\alpha^2+2h_0\alpha\beta+h_0\beta)p^4\\&+4(6b_1\alpha^2+h_1\alpha\beta+h_1\beta)p^3\\&+6\big(\beta h_2+4\alpha^2(b_2+\omega+\sigma^2-\beta\lambda^2-c_2\lambda)\big)p^2\\&-12\beta h_3(\alpha-1)p-12h_4\beta(2\alpha-1)=0.\end{aligned} \tag{14}$$

Setting all the coefficients of Eq. (14) to zero, and then carrying out some routine calculations, we arrive at

$$h_0=-\frac{8b_0\alpha^2}{\beta(2\alpha+1)}, \tag{15}$$

$$h_1=-\frac{6b_1\alpha^2}{\beta(\alpha+1)}, \tag{16}$$

$$h_2=\frac{4\alpha^2(\beta\lambda^2+c_2\lambda-b_2-\omega-\sigma^2)}{\beta}, \tag{17}$$

$$h_3=h_4=0. \tag{18}$$

3. Dynamical properties of Eq. (12)

In this section, we are focused on the analysis of the dynamical properties of ODE (12) fulfilling Eq. (13). To achieve this goal, it is extremely helpful to view the second-order ODE (12) as the Hamiltonian dynamical system

$$\left\{\begin{aligned}p'&=q,\\q'&=h_0p^3+h_1p^2+h_2p,\end{aligned}\right. \tag{19}$$

where the associated Hamiltonian $H(p,q)$ is given by

$$H(p,q)=\frac{h_0}{4}p^4+\frac{h_1}{3}p^3+\frac{h_2}{2}p^2-\frac{1}{2}q^2, \tag{20}$$

in which the constants h_0, h_1, h_2, h_3 and h_4 are given as in Eqs. (15), (16), (17) and (18). For instance, we can gain some insight into nonlinear ODE (12) by contemplating the phase portraits, some of which are shown in Figs. 6–9 of planar Hamiltonian dynamical system (19).

3.1. Stability of the equilibrium points of Hamiltonian system (19)

In this subsection, we shall briefly analyze the equilibrium points of Hamiltonian system (19) and their Lyapunov stability via using some well-known dynamical system theory.[66] For this purpose, let us recall here that for a given point (p,q), the Jacobian matrix associated with dynamical system (19) is given as follows:

$$J_{(p,q)}=\begin{pmatrix}0 & 1\\ 3h_0p^2+2h_1p+h_2 & 0\end{pmatrix}. \tag{21}$$

Let us define

$$\Delta=h_1^2-4h_0h_2,\quad (h_0,h_1,h_2)\in\mathbb{R}^3. \tag{22}$$

It is obvious that if $\Delta>0$ and $h_2\neq 0$, then Hamiltonian system (19) has three equilibrium points:

$$\acute{E}(\acute{p},0),\quad E(0,0),\quad \grave{E}(\grave{q},0), \tag{23}$$

with the constants $\acute{p}$ and $\grave{p}$ given by

$$\acute{p}=\frac{-h_1-\sqrt{\Delta}}{2h_0}=\frac{-h_1-\sqrt{h_1^2-4h_0h_2}}{2h_0}, \tag{24}$$

$$\grave{p}=\frac{-h_1+\sqrt{\Delta}}{2h_0}=\frac{-h_1+\sqrt{h_1^2-4h_0h_2}}{2h_0}. \tag{25}$$

For Hamiltonian system (19), the Jacobian determinants $\det J_{\acute{E}}$, $\det J_E$ and $\det J_{\grave{E}}$ play important roles in analyzing the dynamics near the equilibrium points $\acute{E}$, E and $\grave{E}$, where $\det J_{\acute{E}}$, $\det J_E$ and $\det J_{\grave{E}}$ are given by

$$\det J_{\acute{E}}=\acute{p}\sqrt{\Delta}=\acute{p}\sqrt{h_1^2-4h_0h_2}, \tag{26}$$

$$\det J_E=-h_2, \tag{27}$$

$$\det J_{\grave{E}}=-\grave{p}\sqrt{\Delta}=-\grave{p}\sqrt{h_1^2-4h_0h_2}. \tag{28}$$

Theorem 1 If $h_0\neq 0$, $\Delta>0$ and $h_2\neq 0$ with Δ given by Eq. (22), then Hamiltonian dynamical system (19) has three equilibrium points, that is, $\acute{E}(\acute{p},0)$, $E(0,0)$, $\grave{E}(\grave{q},0)$. In addition, we have:

(i) When $h_0>0$, $h_1>0$ and $h_2>0$, $\acute{E}$ and E are topological saddles, $\grave{E}$ is a center.

(ii) When $h_0>0$, $h_1\in\mathbb{R}$ and $h_2<0$, $\acute{E}$ and $\grave{E}$ are topological saddles, E is a center.

(iii) When $h_0>0$, $h_1<0$ and $h_2>0$, $\acute{E}$ is a center, E and $\grave{E}$ are topological saddles.

(iv) When $h_0<0$, $h_1>0$ and $h_2<0$, $\acute{E}$ and E are centers, $\grave{E}$ is a topological saddle.

(v) When $h_0<0$, $h_1\in\mathbb{R}$ and $h_2>0$, $\acute{E}$ and $\grave{E}$ are centers, E is a topological saddle.

(vi) When $h_0<0$, $h_1<0$ and $h_2<0$, $\acute{E}$ is a topological saddle, E and $\grave{E}$ are centers.

If $h_0\neq 0$, $\Delta=0$ and $h_2\neq 0$ with Δ given by Eq. (22), then the Hamiltonian dynamical system (19) has two equilibrium points, that is, $E(0,0)$, $\tilde{E}(-\frac{h_1}{2h_0},0)$. In addition, we have:

(vii) When $h_0>0$, then E is a topological saddle, $\tilde{E}$ is a cusp.

(viii) When $h_0<0$, then E is a center, $\tilde{E}$ is a cusp.

If $h_0\neq 0$, $h_1\neq 0$ and $h_2=0$, then the Hamiltonian dynamical system (19) has two equilibrium points, that is, $E(0,0)$, $\check{E}(-\frac{h_1}{h_0},0)$. In addition, we have:

(ix) When $h_0>0$, then $\check{E}$ is a topological saddle, E is a cusp.

(x) When $h_0<0$, then $\check{E}$ is a center, E is a cusp.

If $h_0\neq 0$, $h_1=0$ and $h_2=0$, or if $\Delta<0$ with Δ given by Eq. (22), then the Hamiltonian dynamical system (19) has a unique equilibrium point, that is, $E(0,0)$. In addition, we have:

(xi) When $h_0>0$, then E is a topological saddle.

(xii) When $h_0<0$, then E is a center.

Sketchy proof Let us consider the case (i) where $h_0>0$, $h_1>0$ and $h_2>0$. In this situation, the Hamiltonian dynamical system (19) has three equilibrium points, namely, $\acute{E}(\acute{p},0)$, $E(0,0)$, $\grave{E}(\grave{q},0)$. With the aid of Eqs. (26)–(28), we obtain $\det J_{\acute{E}}<0$, $\det J_E<0$ and $\det J_{\grave{E}}>0$. By the Hartman–Grobman theorem and the stable manifold theorem, this, together with $\mathrm{tr}J_{\acute{E}}=\mathrm{tr}J_E=0$, implies that the equilibrium points $\acute{E}$ and E of the dynamical system (19) are saddles. Besides, it is well-known that a non-degenerate equilibrium point of the Hamiltonian dynamical system (19) is either a saddle or a center. We can prove by a contradiction argument that $\grave{E}$ is a center. To this end, we assume, on the contrary, that $\grave{E}$ is not a center, or equivalently, $\grave{E}$ is a saddle. By again applying the Hartman–Grobman theorem and the stable manifold theorem, we can prove that $\det J_{\grave{E}}<0$. This obviously contradicts that $\det J_{\grave{E}}>0$. As a consequence, we conclude that $\grave{E}$ is indeed a center. Cases (ii)–(vi) can be proved in an analogous manner. In summary, cases (i)–(xii) are proved.

We assume in this paragraph that $h_0\neq 0$, $\Delta=0$ and $h_2\neq 0$. The equilibrium point $E(0,0)$ of Hamiltonian dynamical system (19) is non-degenerate and its classification result follows by an argument utilized previously. The equilibrium point $\tilde{E}(-\frac{h_1}{2h_0},0)$ is degenerate. By scrutinizing the phase portrait of dynamical system (19) near the equilibrium point $\tilde{E}(-\frac{h_1}{2h_0},0)$, we conclude that $\tilde{E}$ is a cusp. We can sim-

ilarly prove the result for the case $h_0 \neq 0$, $h_1 \neq 0$ and $h_2 = 0$. Thus, cases (vii)–(x) are proved.

If $\Delta < 0$, then the equilibrium point $E(0,0)$ of Hamiltonian dynamical system (19) is non-degenerate and its classification result follows by an argument utilized previously. Thus, cases (xi)–(xii) are proved.

3.2. Bifurcation analysis of the Hamiltonian system (19)

In this subsection, we shall conduct a brief bifurcation analysis of Hamiltonian system (19) by fixing h_0 and h_1 as nonzero constants, while choosing h_2 as the bifurcation parameter.

For $h_0 > 0$ and $h_1 > 0$, the equilibrium point $\acute{E}(\acute{p},0)$ of the Hamiltonian system (19) remains unstable, the equilibrium points $E(0,0)$ and $\grave{E}(\grave{p},0)$ of the Hamiltonian system (19) (please see Eqs. (24) and (25) for the definitions of $\acute{p}$ and $\grave{p}$, respectively), in contrast, a stability exchange occurs as the parameter h_2 varies across the critical point $h_2 = 0$ in its vicinity; the equilibrium point $E(0,0)$ persists, whereas the equilibrium points $\acute{E}(\acute{p},0)$ and $\grave{E}(\grave{p},0)$ vanish as the parameter h_2 increases across the critical point $h_2 = \frac{h_1^2}{4h_0}$ in its vicinity; consult Fig. 1(a).

For $h_0 > 0$ and $h_1 < 0$, the equilibrium point $\grave{E}(\grave{p},0)$ remains unstable. The equilibrium points $\acute{E}(\acute{p},0)$ and $E(0,0)$, in contrast, alter their stability as the parameter h_2 varies across the critical point $h_2 = 0$ in its vicinity. The equilibrium point $E(0,0)$ persists, whereas the equilibrium points $\acute{E}(\acute{p},0)$ and $\grave{E}(\grave{p},0)$ disappear as the parameter h_2 increases across the critical point $h_2 = \frac{h_1^2}{4h_0}$ in its vicinity; consult Fig. 1(b).

For $h_0 < 0$ and $h_1 > 0$, apart from the equilibrium point $E(0,0)$, the equilibrium points $\acute{E}(\acute{p},0)$ and $\grave{E}(\grave{p},0)$ appear as the parameter h_2 increases across the critical point $h_2 = \frac{h_1^2}{4h_0}$ in its vicinity. The equilibrium point $\acute{E}(\acute{p},0)$ remains stable, the equilibrium points $E(0,0)$ and $\grave{E}(\grave{p},0)$, in contrast, undergo a stability exchange as the parameter h_2 varies across the critical point $h_2 = 0$ in its vicinity; consult Fig. 1(c).

For $h_0 < 0$ and $h_1 < 0$, aside from the equilibrium point $E(0,0)$, the equilibrium points $\acute{E}(\acute{p},0)$ and $\grave{E}(\grave{p},0)$ emerge as the parameter h_2 increases across the critical point $h_2 = \frac{h_1^2}{4h_0}$ in its vicinity. The equilibrium point $\grave{E}(\grave{p},0)$ remains stable, but the equilibrium points $\acute{E}(\acute{p},0)$ and $E(0,0)$, in contrast, switch their stability as the parameter h_2 varies across the critical point $h_2 = 0$ in its vicinity; consult Fig. 1(d).

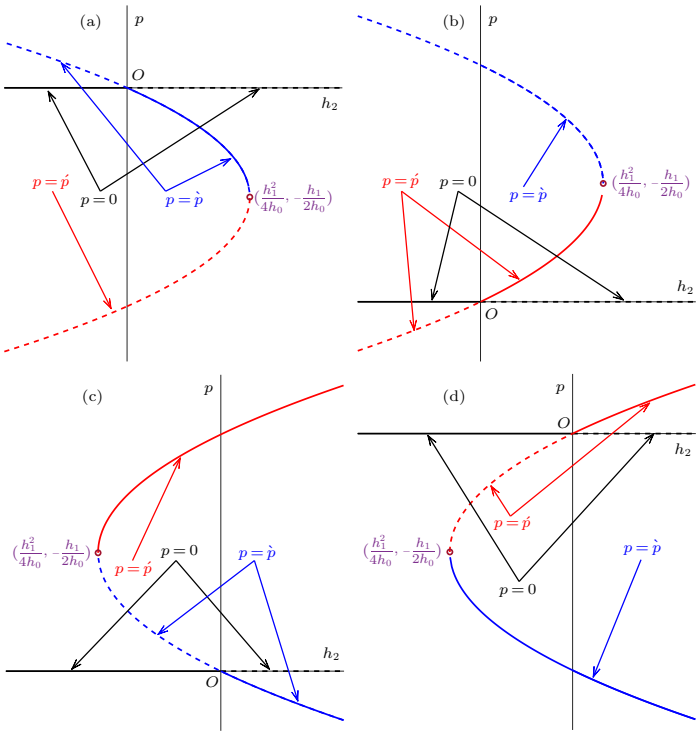


Fig. 1. Bifurcation phenomena of the Hamiltonian system (19) derived from Eqs. (1), (2) and (8) with h_2 as the bifurcation parameter. (a) $h_0 > 0$, $h_1 > 0$; (b) $h_0 > 0$, $h_1 < 0$; (c) $h_0 < 0$, $h_1 > 0$; (d) $h_0 < 0$, $h_1 < 0$.

3.3. Chaos analysis of the Hamiltonian system (19)

In this subsection, we are going to perform a brief chaos analysis of Hamiltonian system (19). To this end, let us introduce the following perturbed Hamiltonian system:

$$\begin{cases} p'(t) = q(t), \\ q'(t) = h_0 p(t)^3 + h_1 p(t)^2 + h_2 p(t) + h_5 \cos(h_6 t), \end{cases} \tag{29}$$

in which $h_5 \cos(h_6 t)$ represents the perturbation term, where the constant h_5 denotes the intensity of the perturbation, and the constant h_6 represents its time frequency. By conducting a series of numerical investigations, we find that the Hamiltonian system (19) can exhibit chaotic dynamical behavior; see Figs. 2–5.

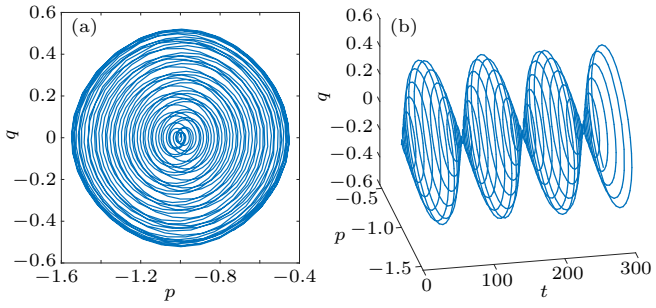


Fig. 2. Visual illustration of chaos in the Hamiltonian system (19). (a) and (b) The orbit (in the phase space) and the state trajectory (in the augmented phase space) of the solution $(p(t),q(t))$, through the point $(-\frac{1001}{1000},0)$, of perturbed Hamiltonian system (29) with $h_0=1$, $h_1=3$, $h_2=2$, $h_5=\frac{23}{787}$ and $h_6=\frac{786}{787}$.

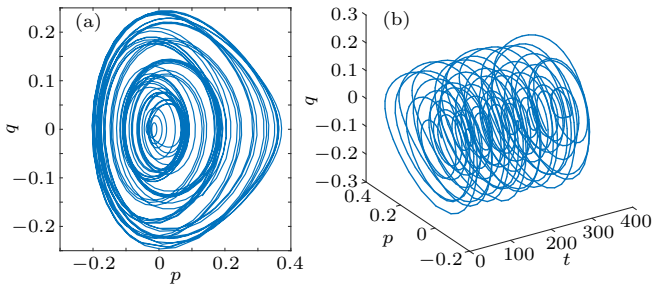


Fig. 3. Visual illustration of chaos in the Hamiltonian system (19). (a) and (b) The orbit and the state trajectory of the solution $(p(t),q(t))$, through the point $(-\frac{39}{1000},\frac{39}{1000})$, of perturbed Hamiltonian system (29) with $h_0=1$, $h_1=\frac{1575}{787}$, $h_2=-\frac{788}{787}$, $h_5=\frac{23}{787}$ and $h_6=\frac{786}{787}$.

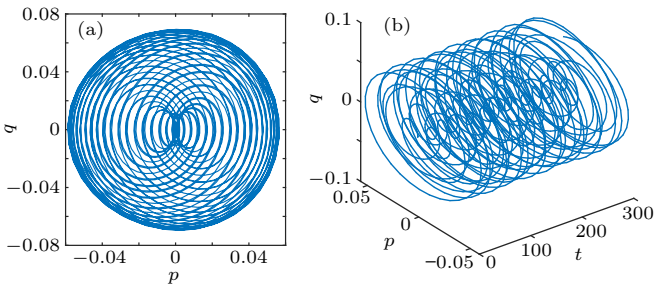


Fig. 4. Visual illustration of chaos in the Hamiltonian system (19). (a) and (b) The orbit and the state trajectory of the solution $(p(t),q(t))$, through the point $(\frac{1}{1000},0)$, of perturbed Hamiltonian system (29) with $h_0=-1$, $h_1=-3$, $h_2=-2$, $h_5=\frac{23}{787}$ and $h_6=\frac{786}{787}$.

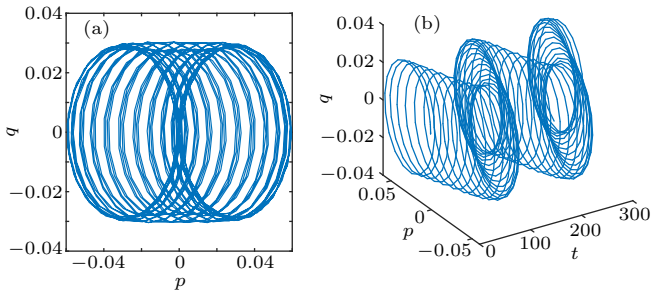


Fig. 5. Visual illustration of chaos in the Hamiltonian system (19). (a) and (b) The orbit and the state trajectory of the solution $(p(t),q(t))$, through the point $(\frac{1}{1000},0)$, of perturbed Hamiltonian system (29) with $h_0=-1$, $h_1=0$, $h_2=0$, $h_5=\frac{23}{787}$ and $h_6=\frac{786}{787}$.

4. Exact solutions of SSLSE (1)

In this section, our principal aim is to find exact solutions to SSLSE (1) based on the analysis on the dynamical behaviors of the planar Hamiltonian dynamical system (19). For the sake of convenience of our later presentation, we introduce as in Eq. (22)

$$\tilde{\Delta}=2h_1^2-9h_0h_2,\quad (h_0,h_1,h_2)\in\mathbb{R}^3, \tag{30}$$

analogously, we introduce respectively $\tilde{p}$ and $\tilde{p}$ by

$$\tilde{p}=\frac{-2h_1-\sqrt{2\tilde{\Delta}}}{3h_0}=\frac{-2h_1-\sqrt{4h_1^2-18h_0h_2}}{3h_0}, \tag{31}$$

$$\tilde{\tilde{p}}=\frac{-2h_1+\sqrt{2\tilde{\Delta}}}{3h_0}=\frac{-2h_1+\sqrt{4h_1^2-18h_0h_2}}{3h_0}. \tag{32}$$

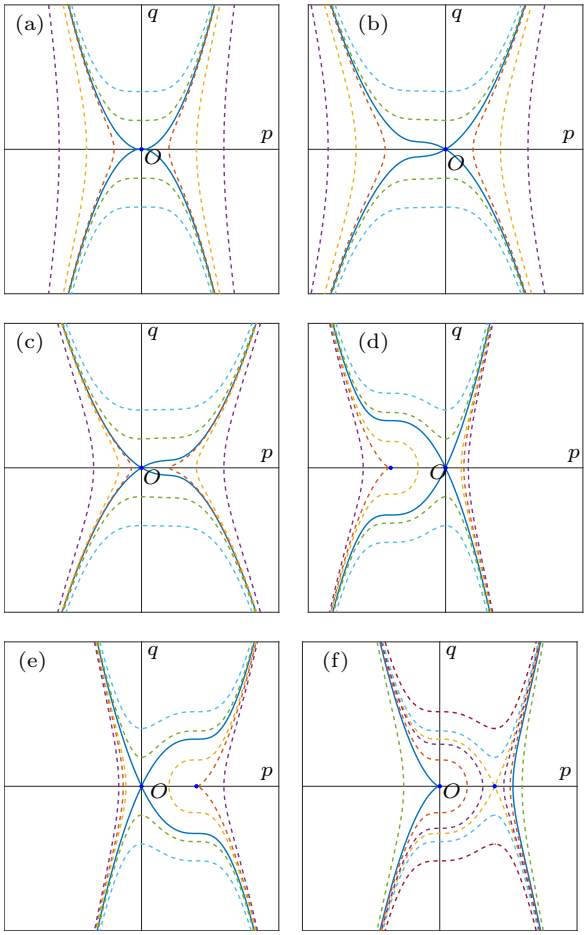


Fig. 6. Phase portrait of the Hamiltonian system (19) derived from Eqs. (1), (2) and (8) with (a) $h_0>0$ and $h_1=h_2=h_3=0$, (b) $h_0>0$, $h_1>0$ and $\Delta<0$, (c) $h_0>0$, $h_1<0$ and $\Delta<0$, (d) $h_0>0$, $h_1>0$ and $\Delta=0$, (e) $h_0>0$, $h_1<0$ and $\Delta=0$, (f) $h_0>0$, $h_1<0$ and $h_2=0$. Consult Eq. (22) for the definition of Δ.

Case 1. $h_0>0$ and $h_1=h_2=h_3=h_4=0$.

In this case, the dynamical system (19) has a unique equilibrium point, namely, $O(0,0)$, and Eq. (13) simplifies to $\pm\frac{p'}{p^2}=\sqrt{\frac{h_0}{2}}$. By scrutinizing Fig. 6(a), we find that the dynamical system (19) has only one exact solution satisfying $p(\xi)>0$ and Eq. (13). Now let us begin to calculate the function $p(\xi)$ corresponding to the solid curve in the first quadrant of the pOq plane. For this purpose, we assume that $\lim\limits_{\xi\to\xi_0^-}p(\xi)=+\infty$. As a result, we have

$$\int_p^{+\infty}\frac{\mathrm{d}u}{u^2}=\sqrt{\frac{h_0}{2}}\int_\xi^{\xi_0}\mathrm{d}\eta,\quad \xi\in(-\infty,\xi_0). \tag{33}$$

After some routine calculations, we have

$$p(\xi)=-\frac{1}{\sqrt{\frac{h_0}{2}}(\xi-\xi_0)},\quad \xi\in(-\infty,\xi_0). \tag{34}$$

Let us calculate the function $p(\xi)$ corresponding to the solid curve in the fourth quadrant of the pOq plane and, as previously, we assume that $\lim\limits_{\xi\to\xi_0^+}p(\xi)=+\infty$. Similar to Eq. (33), we have

$$-\int_{+\infty}^{p}\frac{\mathrm{d}u}{u^2}=\sqrt{\frac{h_0}{2}}\int_{\xi_0}^{\xi}\mathrm{d}\eta,\quad \xi\in(\xi_0,+\infty), \tag{35}$$

or we have equivalently

$$p(\xi)=\frac{1}{\sqrt{\frac{h_0}{2}}(\xi-\xi_0)},\quad \xi\in(\xi_0,+\infty). \tag{36}$$

Combining Eqs. (34) and (36), we arrive at

$$p(\xi)=\frac{1}{\sqrt{\frac{h_0}{2}}|\xi-\xi_0|},\quad \xi\in\mathbb{R}\setminus\{\xi_0\}. \tag{37}$$

This, as well as Eq. (8), implies

$$\Psi_1(\xi)=\left(\frac{h_0}{2}\right)^{-\frac{1}{4\alpha}}|\xi-\xi_0|^{-\frac{1}{2\alpha}},\quad \xi\in\mathbb{R}\setminus\{\xi_0\}. \tag{38}$$

By recalling Eq. (2), we obtain an exact singular solution $\psi_1(x,t)$ of SSLSE (1):

$$\psi_1(x,t)=\left(\frac{2}{h_0}\right)^{\frac{1}{4\alpha}}|x-vt-\xi_0|^{-\frac{1}{2\alpha}}\,\mathrm{e}^{\mathrm{i}(\lambda x-(\omega+\sigma^2)t+\sigma W(t))}. \tag{39}$$

Case 2. $h_0>0$ and $\Delta<0$ with Δ given by Eq. (22).

In this case, the dynamical system (19) has a unique equilibrium point, namely, $O(0,0)$, and it is straightforward to show that $\tilde{\Delta}=\frac{9\Delta-h_1^2}{4}<0$ with $\tilde{\Delta}$ given as in Eq. (30). Based on this finding and by scrutinizing Figs. 6(b) and 6(c), we find that the dynamical system (19) has only one exact solution satisfying $p(\xi)>0$ and Eq. (13). To find the exact solution corresponding to the solid curve in the first quadrant of the pOq plane, assume that $\lim\limits_{\xi\to\xi_0^-}p(\xi)=+\infty$. In analogy with Eq. (33), it follows straightforwardly that

$$\int_{p}^{+\infty}\frac{\mathrm{d}u}{\sqrt{\frac{h_0}{2}u^4+\frac{2h_1}{3}u^3+h_2u^2}}=\int_{\xi}^{\xi_0}\mathrm{d}\eta,$$

which, together with some routine calculations, implies

$$\frac{1}{\sqrt{h_2}}\operatorname{arcsinh}\left(\frac{h_1}{\sqrt{-\frac{\tilde{\Delta}}{2}}}\right)-\frac{1}{\sqrt{h_2}}\operatorname{arcsinh}\left(\frac{3h_2+h_1p}{p\sqrt{-\frac{\tilde{\Delta}}{2}}}\right)=\xi-\xi_0,$$

or, equivalently,

$$p(\xi)=\frac{3h_2}{\sqrt{-\frac{\tilde{\Delta}}{2}}\sinh(\operatorname{arcsinh}\left(\frac{h_1}{\sqrt{-\frac{\tilde{\Delta}}{2}}}\right)+\sqrt{h_2}(\xi_0-\xi))-h_1},$$

$\xi\in(-\infty,\xi_0)$. To find the exact solution corresponding to the solid curve in the fourth quadrant of the pOq plane, assume that $\lim\limits_{\xi\to\xi_0^+}p(\xi)=+\infty$, similar to Eq. (35), we have

$$-\int_{+\infty}^{p}\frac{\mathrm{d}u}{\sqrt{\frac{h_0}{2}u^4+\frac{2h_1}{3}u^3+h_2u^2}}=\int_{\xi_0}^{\xi}\mathrm{d}\eta,$$

which, alongside with some routine calculations, implies

$$p(\xi)=\frac{3h_2}{\sqrt{-\frac{\tilde{\Delta}}{2}}\sinh(\operatorname{arcsinh}\left(\frac{h_1}{\sqrt{-\frac{\tilde{\Delta}}{2}}}\right)+\sqrt{h_2}(\xi-\xi_0))-h_1},$$

$\xi\in(\xi_0,+\infty)$. Therefore, we have

$$p(\xi)=\frac{3h_2}{\sqrt{-\frac{\tilde{\Delta}}{2}}\sinh(\operatorname{arcsinh}\left(\frac{h_1}{\sqrt{-\frac{\tilde{\Delta}}{2}}}\right)+\sqrt{h_2}|\xi-\xi_0|)-h_1},$$

which, as well as Eq. (8), implies

$$\Psi_2(\xi)=\left(\frac{3h_2}{\sqrt{-\frac{\tilde{\Delta}}{2}}\sinh\left(\operatorname{arcsinh}\left(\frac{h_1}{\sqrt{-\frac{\tilde{\Delta}}{2}}}\right)+\sqrt{h_2}|\xi-\xi_0|\right)-h_1}\right)^{\frac{1}{2\alpha}},\quad \xi\in\mathbb{R}\setminus\{\xi_0\}.$$

By recalling Eq. (2), we obtain an exact singular solution $\psi_2(x,t)$ to SSLSE (1):

$$\psi_2(x,t)=\left(\frac{3h_2}{\sqrt{-\frac{\tilde{\Delta}}{2}}\sinh\left(\operatorname{arcsinh}\left(\frac{h_1}{\sqrt{-\frac{\tilde{\Delta}}{2}}}\right)+\sqrt{h_2}|x-vt-\xi_0|\right)-h_1}\right)^{\frac{1}{2\alpha}}\mathrm{e}^{\mathrm{i}(\lambda x-(\omega+\sigma^2)t+\sigma W(t))}. \tag{40}$$

Case 3. $h_0>0$, $\Delta=0$, $h_2\neq0$ with Δ given by Eq. (22).

In this case, the dynamical system (19) has two equilibrium points, namely, $O(0,0)$ and $(-\frac{h_1}{2h_0},0)$, and it is straightforward to show that $\tilde{\Delta}=\frac{9\Delta-h_1^2}{4}<0$ with $\tilde{\Delta}$ given as in Eq. (30). Based on this finding and by scrutinizing Figs. 6(d) and 6(e), we find that the dynamical system (19) has only one exact solution satisfying $p(\xi)>0$ and Eq. (13). By utilizing Eq. (40), we obtain an

exact singular solution $\psi_3(x,t)$ of SSLSE (1) given by

$$\psi_3(x,t)=\left(\frac{6h_2}{\sqrt{2h_0h_2}\sinh(\mathrm{sgn}\,(h_1)\ln(\sqrt{2}+\sqrt{3})+\sqrt{h_2}|x-vt-\xi_0|)-2h_1}\right)^{\frac{1}{2\alpha}}\mathrm{e}^{\mathrm{i}(\lambda x-(\omega+\sigma^2)t+\sigma W(t))},\tag{41}$$

in which the identity $\tilde{\Delta}=2\Delta-h_0h_2=-h_0h_2$ was utilized.

Case 4. $h_0>0$, $h_1<0$ and $h_2=0$.

In this case, the dynamical system (19) has two equilibrium points, namely, $O(0,0)$ and $(-\frac{h_1}{h_0},0)$. By examining Fig. 6(f), we find that the dynamical system (19) has a unique exact solution satisfying $p(\xi)>0$ and Eq. (13). The exact solution corresponds to the solid curve, passing through the point $(-\frac{4h_1}{3h_0},0)$, in the right half of the pOq plane. Based on the above analysis, we have

$$\begin{aligned}&\int_{-\frac{4h_1}{3h_0}}^{p}\frac{\mathrm{d}u}{\sqrt{\frac{h_0}{2}u^4+\frac{2h_1}{3}u^3}}=\int_{\xi_0+\frac{3k\sqrt{2h_0}}{h_1}}^{\xi}\mathrm{d}\eta,\\&\xi\in\left[\xi_0+\frac{3k\sqrt{2h_0}}{h_1},\xi_0+\frac{3k\sqrt{2h_0}}{h_1}-\frac{3\sqrt{2h_0}}{2h_1}\right),\end{aligned}\tag{42}$$

$$\begin{aligned}&-\int_{p}^{-\frac{4h_1}{3h_0}}\frac{\mathrm{d}u}{\sqrt{\frac{h_0}{2}u^4+\frac{2h_1}{3}u^3}}=\int_{\xi}^{\xi_0+\frac{3k\sqrt{2h_0}}{h_1}}\mathrm{d}\eta,\\&\xi\in\left(\xi_0+\frac{3k\sqrt{2h_0}}{h_1}+\frac{3\sqrt{2h_0}}{2h_1},\xi_0+\frac{3k\sqrt{2h_0}}{h_1}\right].\end{aligned}\tag{43}$$

We have by some more routine computations

$$-\frac{3}{h_1}\sqrt{\frac{3h_0p+4h_1}{6p}}=\left|\xi-\xi_0-\frac{3k\sqrt{2h_0}}{h_1}\right|,\tag{44}$$

Or, equivalently, we have

$$\begin{aligned}&p(\xi)=\frac{12h_1}{2h_1^2(\xi-\xi_0-\frac{6k\sqrt{2h_0}}{h_1})^2-9h_0},\\&\xi\in\left(\xi_0+\frac{3k\sqrt{2h_0}}{h_1}+\frac{3\sqrt{2h_0}}{2h_1},\xi_0+\frac{3k\sqrt{2h_0}}{h_1}-\frac{3\sqrt{2h_0}}{2h_1}\right).\end{aligned}\tag{45}$$

Along with Eq. (8), this implies

$$\begin{aligned}&\Psi_4(\xi)=\left(\frac{12h_1}{2h_1^2(\xi-\xi_0-\frac{6k\sqrt{2h_0}}{h_1})^2-9h_0}\right)^{\frac{1}{2\alpha}},\\&\xi\in\left(\xi_0+\frac{3k\sqrt{2h_0}}{h_1}+\frac{3\sqrt{2h_0}}{2h_1},\xi_0+\frac{3k\sqrt{2h_0}}{h_1}-\frac{3\sqrt{2h_0}}{2h_1}\right).\end{aligned}\tag{46}$$

By recalling Eq. (2), we obtain an exact singular and perturbed periodic solution $\psi_4(x,t)$ of SSLSE (1):

$$\begin{aligned}\psi_4(x,t)=&\left(\frac{12h_1}{2h_1^2\left(x-vt-\xi_0-\frac{6k\sqrt{2h_0}}{h_1}\right)^2-9h_0}\right)^{\frac{1}{2\alpha}}\\&\times\mathrm{e}^{\mathrm{i}(\lambda x-(\omega+\sigma^2)t+\sigma W(t))}.\end{aligned}\tag{47}$$

Case 5. $h_0>0$, $h_1>0$ and $h_2=0$.

As with Case 4, the dynamical system (19) has two equilibrium points, namely, $O(0,0)$ and $(-\frac{h_1}{h_0},0)$. By examining Fig. 7(a), we find that the dynamical system (19) has a unique exact solution satisfying $p(\xi)>0$ and Eq. (13) in the right half of the pOq plane. We assume first that $\lim\limits_{\xi\to\xi_0^-}p(\xi)=+\infty$. With this, we have

$$\int_{p}^{+\infty}\frac{\mathrm{d}u}{\sqrt{\frac{h_0}{2}u^4+\frac{2h_1}{3}u^3}}=\int_{\xi}^{\xi_0}\mathrm{d}\eta,\quad\xi\in(-\infty,\xi_0).$$

By some simple calculations, we have immediately

$$\frac{3}{h_1}\sqrt{\frac{h_0}{2}}-\frac{3}{h_1}\sqrt{\frac{3h_0p+4h_1}{6p}}=\xi-\xi_0,\quad\xi\in(-\infty,\xi_0),$$

or, equivalently, we have

$$p(\xi)=\frac{2h_1}{3\left(\left(\frac{h_1}{3}(\xi_0-\xi)+\sqrt{\frac{h_0}{2}}\right)^2-\frac{h_0}{2}\right)},\quad\xi\in(-\infty,\xi_0).\tag{48}$$

We assume now that $\lim\limits_{\xi\to\xi_0^+}p(\xi)=+\infty$ and have similarly

$$-\int_{+\infty}^{p}\frac{\mathrm{d}u}{\sqrt{\frac{h_0}{2}u^4+\frac{2h_1}{3}u^3}}=\int_{\xi_0}^{\xi}\mathrm{d}\eta,\quad\xi\in(\xi_0,+\infty),$$

or, equivalently,

$$p(\xi)=\frac{2h_1}{3\left(\left(\frac{h_1}{3}(\xi-\xi_0)+\sqrt{\frac{h_0}{2}}\right)^2-\frac{h_0}{2}\right)},\quad\xi\in(\xi_0,+\infty).\tag{49}$$

Combining Eqs. (48) and (49), we arrive at

$$p(\xi)=\frac{2h_1}{3\left(\left(\frac{h_1}{3}|\xi-\xi_0|+\sqrt{\frac{h_0}{2}}\right)^2-\frac{h_0}{2}\right)},\quad\xi\in\mathbb{R}\setminus\{\xi_0\}.$$

This, along with Eq. (8), implies

$$\Psi_5(\xi)=\left(\frac{2h_1}{3\left(\left(\frac{h_1}{3}|\xi-\xi_0|+\sqrt{\frac{h_0}{2}}\right)^2-\frac{h_0}{2}\right)}\right)^{\frac{1}{2\alpha}},\quad\xi\in\mathbb{R}\setminus\{\xi_0\}.$$

Using Eq. (2), we get an exact singular solution $\psi_5(x,t)$ to SSLSE (1):

$$\begin{aligned}\psi_5(x,t)=&\left(\frac{2h_1}{3\left(\left(\frac{h_1}{3}|x-vt-\xi_0|+\sqrt{\frac{h_0}{2}}\right)^2-\frac{h_0}{2}\right)}\right)^{\frac{1}{2\alpha}}\\&\times\mathrm{e}^{\mathrm{i}(\lambda x-(\omega+\sigma^2)t+\sigma W(t))}.\end{aligned}\tag{50}$$

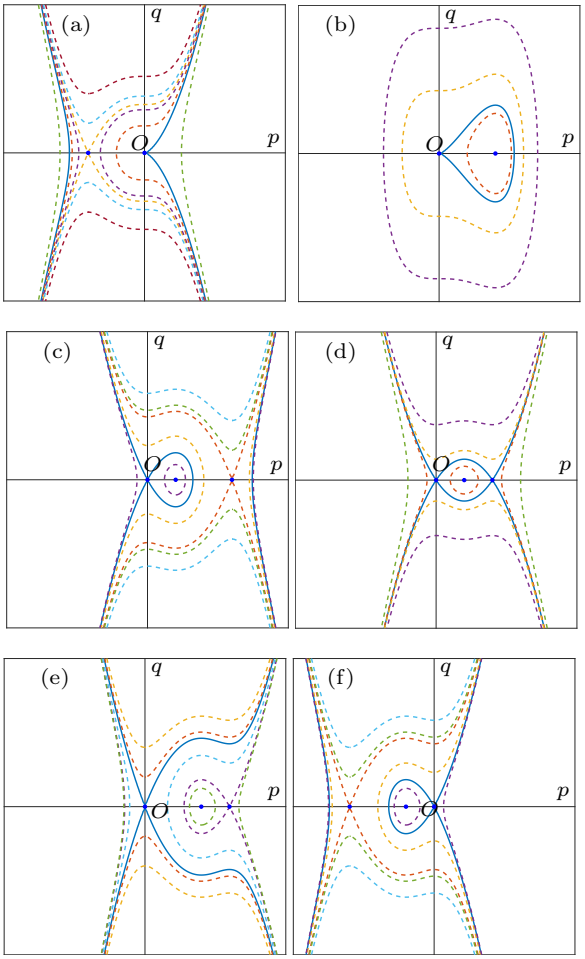


Fig. 7. Phase portrait of the Hamiltonian system (19) derived from Eqs. (1), (2) and (8) with (a) $h_0>0$, $h_1>0$ and $h_2=0$, (b) $h_0<0$, $h_1>0$ and $h_2=0$, (c) $h_0>0$, $h_1<0$ and $\tilde{\Delta}>0$, (d) $h_0>0$, $h_1<0$ and $\tilde{\Delta}=0$, (e) $h_0>0$, $h_1<0$, $\Delta>0$ and $\tilde{\Delta}<0$, (f) $h_0>0$, $h_1>0$ and $\tilde{\Delta}>0$. Consult Eqs. (22) and (30) for the definitions of Δ and $\tilde{\Delta}$, respectively.

Case 6. $h_0<0$, $h_1>0$ and $h_2=0$.

In this case, the dynamical system (19) has two equilibrium points, namely, $O(0,0)$ and $(-\frac{h_1}{h_0},0)$. By examining Fig. 7(b), we infer that dynamical system (19) possesses a unique exact solution that satisfies $p(\xi)>0$ and also meets the conditions of Eq. (13). The exact solution corresponds to the solid curve, passing through the point $(-\frac{4h_1}{3h_0},0)$, in the right half of the the pOq plane. We have by some computations similar to those in Case 4

$$p(\xi)=\frac{12h_1}{2h_1^2(\xi-\xi_0)^2-9h_0},\quad \xi\in\mathbb{R}, \tag{51}$$

$$\Psi_6(\xi)=\left(\frac{12h_1}{2h_1^2(\xi-\xi_0)^2-9h_0}\right)^{\frac{1}{2\alpha}},\quad \xi\in\mathbb{R}, \tag{52}$$

which, together with Eq. (2), yields an exact singular solution $\psi_6(x,t)$ to SSLSE (1):

$$\psi_6(x,t)=\left(\frac{12h_1}{2h_1^2(x-vt-\xi_0)^2-9h_0}\right)^{\frac{1}{2\alpha}}\times \mathrm{e}^{\mathrm{i}(\lambda x-(\omega+\sigma^2)t+\sigma W(t))}. \tag{53}$$

Case 7. $h_0>0$, $h_1<0$, $h_2>0$ and $\tilde{\Delta}>0$ with $\tilde{\Delta}$ given by Eq. (30).

In this case, $\Delta=\frac{4\tilde{\Delta}+h_1^2}{9}>0$ and therefore the dynamical system (19) has three equilibrium points, that is, $E(0,0)$, $(\acute{p},0)$ and $(\grave{p},0)$ with $0<\acute{p}<\tilde{\acute{p}}<\grave{p}<\tilde{\grave{p}}$. By examining Fig. 7(c), we find that dynamical system (19) has two exact solutions that satisfies $p(\xi)>0$ and also meets the condition (13); the exact solutions correspond to the solid curve, passing through the points $(\tilde{\acute{p}},0)$ and $(\tilde{\grave{p}},0)$, respectively, in the right half of the pOq plane. Let us compute the exact solution corresponding to the solid curve passing through the point $(\tilde{\acute{p}},0)$. Assume that $p(\xi_0)=\tilde{\acute{p}}$. We have

$$\int_p^{\tilde{\acute{p}}}\frac{\mathrm{d}u}{\sqrt{\frac{h_0}{2}u^4+\frac{2h_1}{3}u^3+h_2u^2}}=\int_\xi^{\xi_0}\mathrm{d}\eta,\quad \xi\in(-\infty,\xi_0],$$

$$-\int_{\tilde{\acute{p}}}^{p}\frac{\mathrm{d}u}{\sqrt{\frac{h_0}{2}u^4+\frac{2h_1}{3}u^3+h_2u^2}}=\int_{\xi_0}^{\xi}\mathrm{d}\eta,\quad \xi\in[\xi_0,+\infty),$$

which, altogether, imply

$$\frac{1}{\sqrt{h_2}}\operatorname{arccosh}\left(\frac{3h_2+h_1p}{p\sqrt{\frac{\tilde{\Delta}}{2}}}\right)=|\xi-\xi_0|,\quad \xi\in\mathbb{R},$$

or, equivalently,

$$p(\xi)=\frac{3h_2}{\sqrt{\frac{\tilde{\Delta}}{2}}\cosh(\sqrt{h_2}(\xi-\xi_0))-h_1},\quad \xi\in\mathbb{R}.$$

This, along with Eq. (8), implies

$$\Psi_7(\xi)=\left(\frac{3h_2}{\sqrt{\frac{\tilde{\Delta}}{2}}\cosh(\sqrt{h_2}(\xi-\xi_0))-h_1}\right)^{\frac{1}{2\alpha}},\quad \xi\in\mathbb{R}.$$

By recalling Eq. (2), we obtain an exact solution $\psi_7(x,t)$ (corresponding to a perturbed bright soliton) of SSLSE (1):

$$\psi_7(x,t)=\left(\frac{3h_2}{\sqrt{\frac{\tilde{\Delta}}{2}}\cosh(\sqrt{h_2}(x-vt-\xi_0))-h_1}\right)^{\frac{1}{2\alpha}}\times \mathrm{e}^{\mathrm{i}(\lambda x-(\omega+\sigma^2)t+\sigma W(t))}. \tag{54}$$

Let us compute the exact solution corresponding to the solid curve passing through the point $(\tilde{\grave{p}},0)$. Assume that $p(\xi_0)=\tilde{\grave{p}}$. We have

$$-\int_p^{\tilde{\grave{p}}}\frac{\mathrm{d}u}{\sqrt{\frac{h_0}{2}u^4+\frac{2h_1}{3}u^3+h_2u^2}}=\int_\xi^{\xi_0}\mathrm{d}\eta,\quad \xi\in(-\infty,\xi_0].$$

By some routine but tedious calculations, we have immediately

$$\frac{1}{\sqrt{h_2}}\operatorname{arccosh}\left(-\frac{3h_2+h_1p}{p\sqrt{\frac{\tilde{\Delta}}{2}}}\right)=\xi_0-\xi,\quad \xi\in(-\infty,\xi_0],$$

or, equivalently, we have

$$p(\xi)=-\frac{3h_2}{\sqrt{\frac{\tilde{\Delta}}{2}}\cosh(\sqrt{h_2}(\xi-\xi_0))+h_1},\quad \xi\in(-\infty,\xi_0]. \tag{55}$$

In addition, we have

$$\int_{\tilde{p}}^{p}\frac{\mathrm{d}u}{\sqrt{\frac{h_0}{2}u^4+\frac{2h_1}{3}u^3+h_2u^2}}=\int_{\xi_0}^{\xi}\mathrm{d}\eta,\quad \xi\in[\xi_0,+\infty),$$

or, equivalently, we have

$$p(\xi)=-\frac{3h_2}{\sqrt{\frac{\tilde{\Delta}}{2}}\cosh(\sqrt{h_2}(\xi-\xi_0))+h_1},\quad \xi\in[\xi_0,+\infty),$$

which, alongside Eq. (55), implies

$$p(\xi)=-\frac{3h_2}{\sqrt{\frac{\tilde{\Delta}}{2}}\cosh(\sqrt{h_2}(\xi-\xi_0))+h_1},\quad \xi\in\mathbb{R}.$$

This, along with Eq. (8), implies

$$\Psi_8(\xi)=\left(-\frac{3h_2}{\sqrt{\frac{\tilde{\Delta}}{2}}\cosh(\sqrt{h_2}(\xi-\xi_0))+h_1}\right)^{\frac{1}{2\alpha}},\quad \xi\in\mathbb{R}.$$

By recalling Eq. (2), we obtain an exact solution $\psi_8(x,t)$ (corresponding to a perturbed dark soliton) to SSLSE (1):

$$\psi_8(x,t)=\left(-\frac{3h_2}{\sqrt{\frac{\tilde{\Delta}}{2}}\cosh(\sqrt{h_2}(x-vt-\xi_0))+h_1}\right)^{\frac{1}{2\alpha}}\times\mathrm{e}^{\mathrm{i}(\lambda x-(\omega+\sigma^2)t+\sigma W(t))}. \tag{56}$$

Case 8. $h_0>0$, $h_1<0$, $h_2>0$ and $\tilde{\Delta}=0$ with $\tilde{\Delta}$ given by Eq. (30).

In this case, $\Delta=\frac{4\tilde{\Delta}+h_1^2}{9}>0$ and therefore the dynamical system (19) has three equilibrium points, that is, $E(0,0)$, $(\acute{p},0)$ and $(\grave{p},0)$ with $0<\acute{p}<\grave{p}=\tilde{p}=\tilde{p}=-\frac{2h_1}{3h_0}$. By examining Fig. 7(d), we find that dynamical system (19) has three exact solutions that satisfies the conditions $p(\xi)>0$ and Eq. (13). The exact solutions correspond to the solid curves, two of which pass through the points $\left(-\frac{h_1}{3h_0},\frac{h_1^2}{9\sqrt{2h_0^3}}\right)$ and $\left(-\frac{h_1}{3h_0},-\frac{h_1^2}{9\sqrt{2h_0^3}}\right)$, respectively, in the right half of the pOq plane. Let us compute the exact solution corresponding to the solid curve passing through the point $(-\frac{h_1}{3h_0},\frac{h_1^2}{9\sqrt{2h_0^3}})$. Assume that $p(\xi_0)=-\frac{h_1}{3h_0}$. The equation

$$\int_{-\frac{h_1}{3h_0}}^{p}\frac{\mathrm{d}u}{\sqrt{\frac{h_0}{2}u^4+\frac{2h_1}{3}u^3+h_2u^2}}=\int_{\xi_0}^{\xi}\mathrm{d}\eta,\quad \xi\in\mathbb{R} \tag{57}$$

can be reduced to

$$\sqrt{\frac{2}{h_0}}\int_{-\frac{h_1}{3h_0}}^{p}\frac{\mathrm{d}u}{u\left(-\frac{2h_1}{3h_0}-u\right)}=\xi-\xi_0,\quad \xi\in\mathbb{R}, \tag{58}$$

which, as well as some routine calculations, implies

$$\frac{3\sqrt{2h_0}}{h_1}\operatorname{arctanh}\left(\frac{3h_0p+h_1}{h_1}\right)=\xi-\xi_0,\quad \xi\in\mathbb{R}, \tag{59}$$

or, equivalently,

$$p(\xi)=\frac{h_1\tanh\left(\frac{h_1}{3\sqrt{2h_0}}(\xi-\xi_0)\right)-h_1}{3h_0},\quad \xi\in\mathbb{R}. \tag{60}$$

This, along with Eq. (8), implies

$$\Psi_9(\xi)=\left(\frac{h_1\tanh\left(\frac{h_1}{3\sqrt{2h_0}}(\xi-\xi_0)\right)-h_1}{3h_0}\right)^{\frac{1}{2\alpha}},\quad \xi\in\mathbb{R}. \tag{61}$$

By recalling Eq. (2), we obtain an exact solution $\psi_9(x,t)$ (corresponding to a perturbed dark soliton) to SSLSE (1):

$$\psi_9(x,t)=\left(\frac{h_1\tanh\left(\frac{h_1}{3\sqrt{2h_0}}(x-vt-\xi_0)\right)-h_1}{3h_0}\right)^{\frac{1}{2\alpha}}\times\mathrm{e}^{\mathrm{i}(\lambda x-(\omega+\sigma^2)t+\sigma W(t))}. \tag{62}$$

Let us compute the exact solution corresponding to the solid curve passing through the point $\left(-\frac{h_1}{3h_0},-\frac{h_1^2}{9\sqrt{2h_0^3}}\right)$. To this end, we assume that $p(\xi_0)=-\frac{h_1}{3h_0}$. We have

$$-\int_{-\frac{h_1}{3h_0}}^{p}\frac{\mathrm{d}u}{\sqrt{\frac{h_0}{2}u^4+\frac{2h_1}{3}u^3+h_2u^2}}=\int_{\xi_0}^{\xi}\mathrm{d}\eta,\quad \xi\in\mathbb{R},$$

or, equivalently, we have

$$p(\xi)=-\frac{h_1\tanh\left(\frac{h_1}{3\sqrt{2h_0}}(\xi-\xi_0)\right)+h_1}{3h_0},\quad \xi\in\mathbb{R}. \tag{63}$$

Combining Eqs. (8) and (63), we arrive at

$$\Psi_{14}(\xi)=\left(-\frac{h_1\tanh\left(\frac{h_1}{3\sqrt{2h_0}}(\xi-\xi_0)\right)+h_1}{3h_0}\right)^{\frac{1}{2\alpha}},\quad \xi\in\mathbb{R}.$$

By recalling Eq. (2), we obtain an exact solution $\psi_{10}(x,t)$ (corresponding to a perturbed dark soliton) to SSLSE (1):

$$\psi_{10}(x,t)=\left(-\frac{h_1\tanh\left(\frac{h_1}{3\sqrt{2h_0}}(x-vt-\xi_0)\right)+h_1}{3h_0}\right)^{\frac{1}{2\alpha}}\times\mathrm{e}^{\mathrm{i}(\lambda x-(\omega+\sigma^2)t+\sigma W(t))}. \tag{64}$$

Let us compute the exact solution corresponding to the solid curve in the half plane $p\geqslant-\frac{2h_1}{3h_0}$. We assume now that $\lim\limits_{\xi\to\xi_0^-}p(\xi)=+\infty$. The following expression

$$\int_{p}^{+\infty}\frac{\mathrm{d}u}{\sqrt{\frac{h_0}{2}u^4+\frac{2h_1}{3}u^3+h_2u^2}}=\int_{\xi}^{\xi_0}\mathrm{d}\eta,\quad \xi\in(-\infty,\xi_0),$$

simplifies to

$$-\sqrt{\frac{2}{h_0}}\int_{p}^{+\infty}\frac{\mathrm{d}u}{u(\frac{2h_1}{3h_0}+u)}=\int_{\xi}^{\xi_0}\mathrm{d}\eta,\quad \xi\in(-\infty,\xi_0),$$

which, together with some routine calculations, implies

$$-\frac{3\sqrt{2h_0}}{h_1}\operatorname{arctanh}\left(\frac{h_1}{3h_0p+h_1}\right)=\xi_0-\xi,\quad \xi\in(-\infty,\xi_0),$$

or, equivalently,

$$p(\xi)=-\frac{h_1\coth\left(\frac{h_1}{3\sqrt{2h_0}}(\xi_0-\xi)\right)+h_1}{3h_0},\quad \xi\in(-\infty,\xi_0). \tag{65}$$

We assume that $\lim\limits_{\xi\to\xi_0^+}p(\xi)=+\infty$. The following expression

$$\begin{aligned}&\int_{+\infty}^{p}\frac{-\mathrm{d}u}{\sqrt{\frac{h_0}{2}u^4+\frac{2h_1}{3}u^3+h_2u^2}}=\sqrt{\frac{2}{h_0}}\int_{+\infty}^{p}\frac{\mathrm{d}u}{u\left(\frac{2h_1}{3h_0}+u\right)}\\&=\int_{\xi_0}^{\xi}\mathrm{d}\eta,\quad \xi\in(\xi_0,+\infty),\end{aligned}$$

can be converted into

$$p(\xi)=-\frac{h_1\coth\left(\frac{h_1}{3\sqrt{2h_0}}(\xi-\xi_0)\right)+h_1}{3h_0},\quad \xi\in(\xi_0,+\infty),$$

which, together with Eq. (65), implies

$$p(\xi)=-\frac{h_1\coth\left(\frac{h_1}{3\sqrt{2h_0}}|\xi-\xi_0|\right)+h_1}{3h_0},\quad \xi\in\mathbb{R}\setminus\{\xi_0\}.$$

This, along with Eq. (8), implies

$$\Psi_{11}(\xi)=\left(-\frac{h_1\coth\left(\frac{h_1}{3\sqrt{2h_0}}|\xi-\xi_0|\right)+h_1}{3h_0}\right)^{\frac{1}{2\alpha}},\quad \xi\in\mathbb{R}\setminus\{\xi_0\}.$$

By recalling Eq. (2), we obtain an exact singular solution $\psi_{11}(x,t)$ to SSLSE (1):

$$\begin{aligned}\psi_{11}(x,t)=&\left(-\frac{h_1\coth\left(\frac{h_1}{3\sqrt{2h_0}}|x-vt-\xi_0|\right)+h_1}{3h_0}\right)^{\frac{1}{2\alpha}}\\&\times\mathrm{e}^{\mathrm{i}(\lambda x-(\omega+\sigma^2)t+\sigma W(t))}.\end{aligned}\tag{66}$$

Case 9. $h_0>0$, $h_1<0$, $h_2>0$ and $\Delta\tilde{\Delta}<0$ with Δ and $\tilde{\Delta}$ given by Eqs. (22) and (30), respectively.

In this case, $\tilde{\Delta}<0<\Delta$ and therefore dynamical system (19) has three equilibrium points, that is, $E(0,0)$, $(\acute{p},0)$ and $(\grave{p},0)$ with $0<\acute{p}<\grave{p}$. By scrutinizing Fig. 7(e), we conclude that dynamical system (19) has only one exact solution that satisfies $p(\xi)>0$ and also meets the condition (13) in the right half of the pOq plane. By mimicking the calculations in Case 2, we can obtain an exact solution $\psi_2(x,t)$ to SSLSE (1) given by Eq. (40).

Case 10. $h_0>0$, $h_1>0$, $h_2>0$ and $\tilde{\Delta}>0$ with $\tilde{\Delta}$ given by Eq. (30).

In this case, $\Delta=\frac{4\tilde{\Delta}+h_1^2}{9}>0$ and therefore dynamical system (19) has three equilibrium points: $E(0,0)$, $(\acute{p},0)$, and $(\grave{p},0)$, where $\acute{p}<\grave{p}<0$. By examining closely Fig. 7(f), we conclude that dynamical system (19) has a unique exact solution that satisfies $p(\xi)>0$ and the restriction (13) in the right half of the pOq plane. We assume that $\lim\limits_{\xi\to\xi_0^-}p(\xi)=+\infty$. We immediately have

$$\int_{p}^{+\infty}\frac{\mathrm{d}u}{\sqrt{\frac{h_0}{2}u^4+\frac{2h_1}{3}u^3+h_2u^2}}=\int_{\xi}^{\xi_0}\mathrm{d}\eta,\quad \xi\in(-\infty,\xi_0),$$

which, together with some routine computations, implies

$$\frac{1}{\sqrt{h_2}}\operatorname{arccosh}\left(\frac{3h_2+h_1p}{p\sqrt{\frac{\tilde{\Delta}}{2}}}\right)-\frac{1}{\sqrt{h_2}}\operatorname{arccosh}\left(\frac{h_1}{\sqrt{\frac{\tilde{\Delta}}{2}}}\right)=\xi_0-\xi,$$

or, equivalently,

$$p(\xi)=\frac{3h_2}{\sqrt{\frac{\tilde{\Delta}}{2}}\cosh\left(\sqrt{h_2}(\xi_0-\xi)+\operatorname{arccosh}\left(\frac{h_1}{\sqrt{\frac{\tilde{\Delta}}{2}}}\right)\right)-h_1},\tag{67}$$

$\xi\in(-\infty,\xi_0)$. We now assume that $\lim\limits_{\xi\to\xi_0^+}p(\xi)=+\infty$ and have

$$-\int_{+\infty}^{p}\frac{\mathrm{d}u}{\sqrt{\frac{h_0}{2}u^4+\frac{2h_1}{3}u^3+h_2u^2}}=\int_{\xi_0}^{\xi}\mathrm{d}\eta,$$

which can be transformed into

$$p(\xi)=\frac{3h_2}{\sqrt{\frac{\tilde{\Delta}}{2}}\cosh\left(\sqrt{h_2}(\xi-\xi_0)+\operatorname{arccosh}\left(\frac{h_1}{\sqrt{\frac{\tilde{\Delta}}{2}}}\right)\right)-h_1},\tag{68}$$

$\xi\in(\xi_0,+\infty)$. Combining Eqs. (67) and (68) yields

$$p(\xi)=\frac{3h_2}{\sqrt{\frac{\tilde{\Delta}}{2}}\cosh\left(\sqrt{h_2}|\xi-\xi_0|+\operatorname{arccosh}\left(\frac{h_1}{\sqrt{\frac{\tilde{\Delta}}{2}}}\right)\right)-h_1},$$

$\xi\in\mathbb{R}\setminus\{\xi_0\}$. This, along with Eq. (8), implies

$$\Psi_{12}(\xi)=\left(\frac{3h_2}{\sqrt{\frac{\tilde{\Delta}}{2}}\cosh\left(\sqrt{h_2}|\xi-\xi_0|+\operatorname{arccosh}\left(\frac{h_1}{\sqrt{\frac{\tilde{\Delta}}{2}}}\right)\right)-h_1}\right)^{\frac{1}{2\alpha}},\quad \xi\in\mathbb{R}\setminus\{\xi_0\}.$$

By recalling Eq. (2), we obtain an exact singular solution $\psi_{12}(x,t)$ to SSLSE (1):

$$\psi_{12}(x,t)=\left(\frac{3h_2}{\sqrt{\frac{\tilde{\Delta}}{2}}\cosh\left(\sqrt{h_2}|x-vt-\xi_0|+\operatorname{arccosh}\left(\frac{h_1}{\sqrt{\frac{\tilde{\Delta}}{2}}}\right)\right)-h_1}\right)^{\frac{1}{2\alpha}}\mathrm{e}^{\mathrm{i}(\lambda x-(\omega+\sigma^2)t+\sigma W(t))}.\tag{69}$$

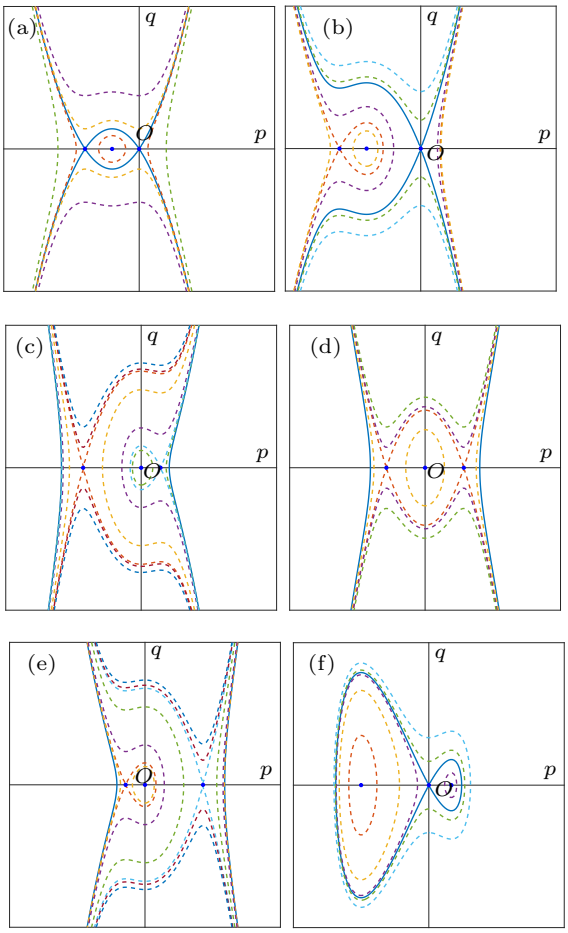


Fig. 8. Phase portrait of the Hamiltonian system (19) derived from Eqs. (1), (2) and (8) with (a) $h_0>0$, $h_1>0$ and $\tilde{\Delta}=0$, (b) $h_0>0$, $h_1>0$ and $\tilde{\Delta}<0$, (c) $h_0>0$, $h_1>0$ and $h_2<0$, (d) $h_0>0$, $h_1=0$ and $h_2<0$, (e) $h_0>0$, $h_1<0$ and $h_2<0$, (f) $h_0<0$, $h_1<0$ and $h_2>0$. Consult Eqs. (22) and (30) for the definitions of Δ and $\tilde{\Delta}$, respectively.

Case 11. $h_0>0$, $h_1>0$, $h_2>0$ and $\tilde{\Delta}=0$ with $\tilde{\Delta}$ given by Eq. (30).

In this case, $\Delta=\frac{4\tilde{\Delta}+h_1^2}{9}>0$ and therefore dynamical system (19) has three equilibrium points: $E(0,0)$, $(\acute{p},0)$, and $(\grave{p},0)$, where $\acute{p}<\grave{p}<0$. By closely examining Fig. 8(a), we conclude that dynamical system (19) has a unique exact solution that satisfies $p(\xi)>0$ and the restriction (13) in the right half of the pOq plane. We assume that $\lim\limits_{\xi\to\xi_0^-}p(\xi)=+\infty$. The following expression

$$\int_p^{+\infty}\frac{\mathrm{d}u}{\sqrt{\frac{h_0}{2}u^4+\frac{2h_1}{3}u^3+h_2u^2}}=\int_\xi^{\xi_0}\mathrm{d}\eta,\quad \xi\in(-\infty,\xi_0),$$

simplifies to

$$\sqrt{\frac{2}{h_0}}\int_p^{+\infty}\frac{\mathrm{d}u}{u\left(\frac{2h_1}{3h_0}+u\right)}=\int_\xi^{\xi_0}\mathrm{d}\eta,\quad \xi\in(-\infty,\xi_0),$$

which, together with some routine calculations, implies

$$\frac{3\sqrt{2h_0}}{h_1}\operatorname{arctanh}\left(\frac{h_1}{3h_0p+h_1}\right)=\xi_0-\xi,\quad \xi\in(-\infty,\xi_0),$$

or, equivalently,

$$p(\xi)=\frac{h_1\coth\left(\frac{h_1}{3\sqrt{2h_0}}(\xi_0-\xi)\right)-h_1}{3h_0},\quad \xi\in(-\infty,\xi_0). \tag{70}$$

We assume that $\lim\limits_{\xi\to\xi_0^+}p(\xi)=+\infty$. The following expression

$$-\int_{+\infty}^p\frac{\mathrm{d}u}{\sqrt{\frac{h_0}{2}u^4+\frac{2h_1}{3}u^3+h_2u^2}}=\int_{\xi_0}^{\xi}\mathrm{d}\eta,\quad \xi\in(\xi_0,+\infty),$$

can be converted into

$$p(\xi)=\frac{h_1\coth\left(\frac{h_1}{3\sqrt{2h_0}}(\xi-\xi_0)\right)-h_1}{3h_0},\quad \xi\in(\xi_0,+\infty).$$

This, along with Eq. (70), implies

$$p(\xi)=\frac{h_1\coth\left(\frac{h_1}{3\sqrt{2h_0}}|\xi-\xi_0|\right)-h_1}{3h_0},\quad \xi\in\mathbb{R}\setminus\{\xi_0\}.$$

Thanks to Eq. (8), this implies further that

$$\Psi_{13}(\xi)=\left(\frac{h_1\coth\left(\frac{h_1}{3\sqrt{2h_0}}|\xi-\xi_0|\right)-h_1}{3h_0}\right)^{\frac{1}{2\alpha}},\quad \xi\in\mathbb{R}.$$

We thus obtain an exact singular solution $\psi_{13}(x,t)$ to SSLSE (1):

$$\psi_{13}(x,t)=\left(\frac{h_1\coth\left(\frac{h_1}{3\sqrt{2h_0}}|x-vt-\xi_0|\right)-h_1}{3h_0}\right)^{\frac{1}{2\alpha}}\times\mathrm{e}^{\mathrm{i}(\lambda x-(\omega+\sigma^2)t+\sigma W(t))}. \tag{71}$$

Case 12. $h_0>0$, $h_1>0$, $h_2>0$ and $\Delta\tilde{\Delta}<0$ with Δ and $\tilde{\Delta}$ given by Eqs. (22) and (30), respectively.

In this case, $\tilde{\Delta}<0<\Delta$ and therefore dynamical system (19) has three equilibrium points, namely, $E(0,0)$, $(\acute{p},0)$ and $(\grave{p},0)$ with $\acute{p}<\grave{p}<0$. By scrutinizing Fig. 8(b), we conclude that dynamical system (19) has solely one exact solution that satisfies $p(\xi)>0$ and meets condition (13) in the right half of the pOq plane. By following the calculations in Case 2, we can obtain the exact solution $\psi_2(x,t)$ to SSLSE (1), given by Eq. (40).

Case 13. $h_0>0$, $h_1\in\mathbb{R}$ and $h_2<0$.

In this case, the dynamical system (19) has three equilibrium points, i.e., $E(0,0)$, $(\acute{p},0)$ and $(\grave{p},0)$ with $\tilde{p}<\acute{p}<0<\grave{p}<\tilde{p}$. By contemplating Figs. 8(c)–8(e), we find that dynamical system (19) possesses a unique exact solution that satisfies $p(\xi)>0$ and Eq. (13). The exact solution corresponds to the solid curve passing through the point $(\tilde{p},0)$ in the right half of the pOq plane. We assume now that $p(\xi_0)=\tilde{p}$. We immediately have

$$\int_{\tilde{p}}^p\frac{\mathrm{d}u}{\sqrt{\frac{h_0}{2}u^4+\frac{2h_1}{3}u^3+h_2u^2}}=\int_{\xi_0}^{\xi}\mathrm{d}\eta,\quad \xi\in[\xi_0,+\infty),$$

which, along with some calculations, implies

$$\frac{\pi}{\sqrt{-h_2}}-\frac{1}{\sqrt{-h_2}}\arccos\left(\frac{3h_2+h_1p}{p\sqrt{\frac{\Delta}{2}}}\right)=\xi-\xi_0,$$

$$\xi \in [\xi_0, +\infty),$$

or, equivalently,

$$p(\xi) = -\frac{3h_2}{\sqrt{\frac{\tilde{\Delta}}{2}}\cos(\sqrt{-h_2}(\xi-\xi_0))+h_1}, \quad \xi \in [\xi_0, +\infty). \tag{72}$$

Analogously, we have

$$-\int_p^{\tilde{p}} \frac{\mathrm{d}u}{\sqrt{\frac{h_0}{2}u^4+\frac{2h_1}{3}u^3+h_2u^2}} = \int_\xi^{\xi_0} \mathrm{d}\eta, \quad \xi \in (-\infty, \xi_0],$$

which can be transformed into

$$p(\xi) = -\frac{3h_2}{\sqrt{\frac{\tilde{\Delta}}{2}}\cos(\sqrt{-h_2}(\xi_0-\xi))+h_1}, \quad \xi \in (-\infty, \xi_0]. \tag{73}$$

Combining Eqs. (72) and (73), we obtain

$$p(\xi) = -\frac{3h_2}{\sqrt{\frac{\tilde{\Delta}}{2}}\cos(\sqrt{-h_2}(\xi-\xi_0))+h_1}, \quad \xi \in \mathbb{R}.$$

By virtue of Eq. (8), this implies

$$\Psi_{14}(\xi) = \left(\frac{-3h_2}{\max\left(0, \sqrt{\frac{\tilde{\Delta}}{2}}\cos(\sqrt{-h_2}(\xi-\xi_0))+h_1\right)}\right)^{\frac{1}{2\alpha}}, \quad \xi \in \mathbb{R}.$$

By recalling Eq. (2), we obtain an exact singular and perturbed periodic solution $\psi_{14}(x,t)$ to SSLSE (1):

$$\psi_{14}(x,t) = \left(\frac{-3h_2}{\max\left(0, \sqrt{\frac{\tilde{\Delta}}{2}}\cos(\sqrt{-h_2}(x-vt-\xi_0))+h_1\right)}\right)^{\frac{1}{2\alpha}} \times \mathrm{e}^{\mathrm{i}(\lambda x-(\omega+\sigma^2)t+\sigma W(t))}. \tag{74}$$

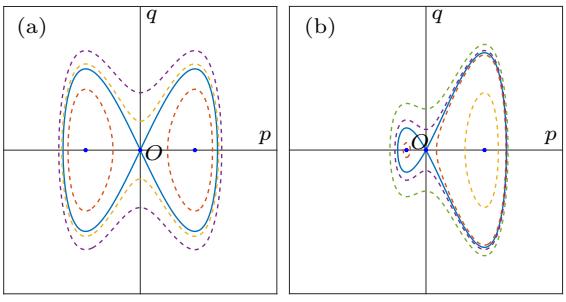


Fig. 9. Phase portrait of the Hamiltonian system (19) derived from Eqs. (1), (2) and (8) with (a) $h_0 < 0$, $h_1 = 0$ and $h_2 > 0$, (b) $h_0 < 0$, $h_1 > 0$ and $h_2 > 0$.

Case 14. $h_0 < 0$, $h_1 \in \mathbb{R}$ and $h_2 > 0$.

In this case, dynamical system (19) has three equilibrium points; that is, $E(0,0)$, $(\acute{p},0)$ and $(\grave{p},0)$ with $\tilde{p} < \grave{p} < 0 < \acute{p} < \tilde{\acute{p}}$. By closely examining Figs. 8(f) and 9(a), 9(b), we conclude that dynamical system (19) admits a unique exact solution that satisfies $p(\xi) > 0$ and meets the condition of Eq. (13); the exact solution corresponds to the solid curve, passing through the point $(\tilde{\acute{p}},0)$, in the right half of the pOq plane. By performing calculations as in Case 7, we can obtain the exact solution $\psi_7(x,t)$ to SSLSE (1) given by Eq. (54).

Remark 2 We find all possible exact solutions, i.e., ψ_k $(k = 1,2,\ldots,14)$ given by Eqs. (39), (40), (41), (47), (50), (53), (54), (56), (62), (64), (66), (69), (71) and (74), to SSLSE (1) by examining the dynamical properties of the previously introduced auxiliary Hamiltonian system (19). Here by 'all', we mean the totality of the exact solutions to SSLSE (1) satisfying the additional restriction (12). Furthermore, we can obtain visual clues to determine the exact solutions ψ_k $(k = 1,2,\ldots,14)$ by examining the phase portraits of Hamiltonian system (19), i.e., Figs. 6–9.

Remark 2 Our obtained exact solutions to SSLSE (1) can be classified into singular solutions, periodic solutions, and perturbed bright as well as dark solitons. For example, ψ_2 given by Eq. (40) is a singular solution, ψ_7 given by Eq. (54) represents a perturbed bright soliton, ψ_9 given by Eq. (62) represents a perturbed dark soliton, ψ_{14} given by Eq. (74) is a periodic solution.

5. Numerical simulations

In Section 4, we obtained four types of exact solutions to SSLSE (1) and noted that they can be classified into four groups. In this section, we aim to visualize a representative example from each type and illustrate the impact of stochastic perturbation on the exact solutions. To this end, we compute specific exact solutions $\hat{\psi}_2(x,t)$, $\hat{\psi}_7(x,t)$, $\hat{\psi}_9(x,t)$ and $\hat{\psi}_{14}(x,t)$, in the forms (40), (54), (62) and (74), respectively, to SSLSE (1). Accordingly, we present graphs of the specific exact solutions mentioned above.

Let us fix $b_0 = -2/27$, $b_1 = -55/459$, $b_2 = -247/108$, $c_0 = c_1 = c_3 = 0$, $c_2 = -1$, $\alpha = 3/2$ and $\beta = 1$, we have by some computations that $h_0 = 1/3$, $h_1 = 11/17$, $h_2 = 1/3$, $h_3 = h_4 = 0$, $\xi_0 = -2$, $\sigma = 1$, $\lambda = 1$, $\omega = 1$ and $v = 1$. With the help of these parameters, we can obtain by some calculations that

$$\hat{\Psi}_2(\xi) = \frac{\sqrt[6]{108664}}{\sqrt[3]{\sinh\left(\operatorname{arcsinh}\left(\frac{11\sqrt{94}}{47}\right)+\frac{\sqrt{3}}{3}|\xi+2|\right)-\frac{22}{\sqrt{94}}}}. \tag{75}$$

Recall Eq. (40), we obtain

$$\begin{aligned}\hat{\psi}_2(x,t) &= \hat{\Psi}_2(x-t)\,\mathrm{e}^{\mathrm{i}(x-2t+W(t))} \\ &= \frac{\sqrt[6]{108664}}{\sqrt[3]{\sinh(\operatorname{arcsinh}(\frac{11\sqrt{94}}{47})+\frac{\sqrt{3}}{3}|x-t+2|)-\frac{22}{\sqrt{94}}}} \\ &\quad \times \mathrm{e}^{\mathrm{i}(x-2t+W(t))}.\end{aligned} \tag{76}$$

Please consult Fig. 10 for the graph of $\hat{\Psi}_2(\xi)$ and $\hat{\psi}_2(x,t)$.

Let us fix $b_0 = -2/9$, $b_1 = 20/27$, $b_2 = -7/3$, $c_0 = c_1 = c_3 = 0$, $c_2 = -1$, $\alpha = 3/2$ and $\beta = 1$, we have by some calculations that $h_0 = 1$, $h_1 = -4$, $h_2 = 3$, $h_3 = h_4 = 0$, $\xi_0 = -15/2$, $\sigma = 1$, $\lambda = 1$, $\omega = 1$ and $v = 1$. With these parameters at our disposal, we can get

$$\hat{\Psi}_7(\xi) = \frac{\sqrt[6]{3240}}{\sqrt[3]{\cosh(\sqrt{3}(\xi+\frac{15}{2}))+\frac{8}{\sqrt{10}}}}; \tag{77}$$

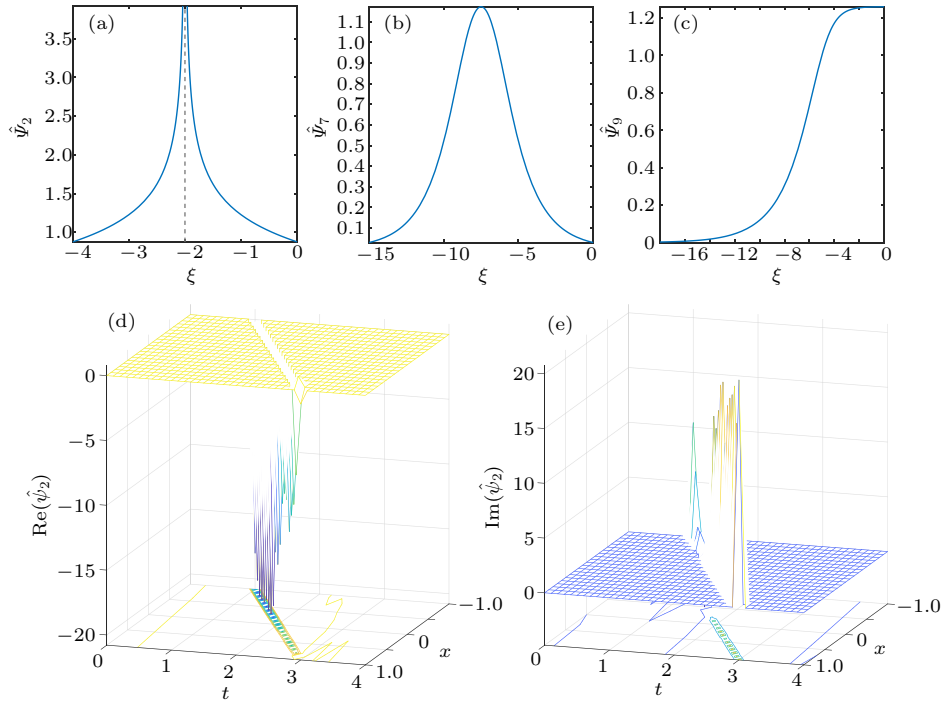


Fig. 10. Visualization of $\hat{\Psi}_2$, $\hat{\Psi}_7$, $\hat{\Psi}_9$ and $\hat{\psi}_2$ given in Eqs. (75), (77), (79) and (76), respectively. (a) The graph of $\mathrm{Re}(\hat{\psi}_2)$. (b) The graph of $\hat{\Psi}_7$. (c) The graph of $\hat{\Psi}_9$. (d) The graph of $\mathrm{Im}(\hat{\psi}_2)$. (e) The graph of $\hat{\Psi}_2$.

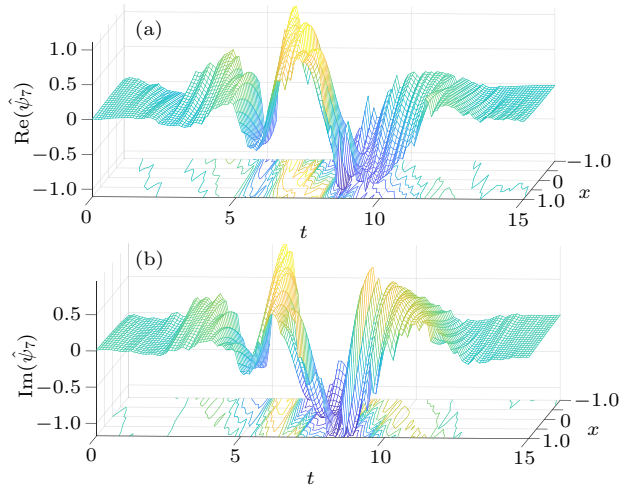


Fig. 11. Visualization of the specific solution $\hat{\psi}_7$ given by Eq. (78). (a) The graph of $\mathrm{Re}(\hat{\psi}_7)$. (b) The graph of $\mathrm{Im}(\hat{\psi}_7)$.

see Fig. 10(b) for its visualization. By recalling Eq. (54), we obtain (see Fig. 11 for its visualization)

$$\hat{\psi}_7(x,t)=\frac{\sqrt[6]{3240}}{\sqrt[3]{\cosh(\sqrt{3}(x-t+\frac{15}{2}))+\frac{8}{\sqrt{10}}}}\,\mathrm{e}^{\mathrm{i}(x-2t+W(t))}. \quad (78)$$

Let us fix $b_0=-2/9$, $b_1=5/9$, $b_2=-89/36$, $c_0=c_1=c_3=0$, $c_2=-1$, $\alpha=3/2$ and $\beta=1$, we have by some computations that $h_0=1$, $h_1=-3$, $h_2=2$, $h_3=h_4=0$, $\xi_0=-5$, $\sigma=1$, $\lambda=1$, $\omega=1$ and $v=1$. What's more, we have

$$\hat{\Psi}_9(\xi)=\sqrt[3]{1+\tanh\left(\frac{\xi+5}{\sqrt{2}}\right)}; \quad (79)$$

see Fig. 10(c) for its visualization. By recalling Eq. (62), we obtain (see Fig. 12 for its visualization)

$$\hat{\psi}_9(x,t)=\sqrt[3]{1+\tanh\left(\frac{x-t+5}{\sqrt{2}}\right)}\,\mathrm{e}^{\mathrm{i}(x-2t+W(t))}. \quad (80)$$

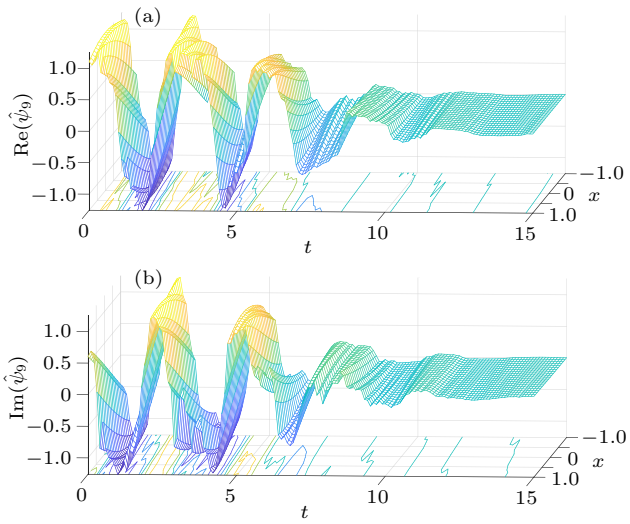


Fig. 12. Visualization of $\hat{\psi}_9$ given by Eq. (80). (a) The graph of $\mathrm{Re}(\hat{\psi}_9)$. (b) The graph of $\mathrm{Im}(\hat{\psi}_9)$.

Let us fix $b_0=-2/9$, $b_1=-10/27$, $b_2=-5/3$, $c_0=c_1=c_3=0$, $c_2=-1$, $\alpha=3/2$ and $\beta=1$, we have by some computations that $h_0=1$, $h_1=2$, $h_2=-3$, $h_3=h_4=0$, $\xi_0=-5$, $\sigma=1$, $\lambda=1$, $\omega=1$ and $v=1$. In addition, we can get the profile

$$\hat{\Psi}_{14}(\xi)=\sqrt[3]{\frac{18}{\max(0,\sqrt{70}\cos(\sqrt{3}(\xi+5))+4)}}. \quad (81)$$

By recalling Eq. (74), we obtain (see Fig. 13 for its visualiza-

tion)

$$\begin{aligned}\hat{\psi}_{14}(x,t) &= \hat{\Psi}_{14}(x-t)\,\mathrm{e}^{\mathrm{i}(x-2t+W(t))}\\ &= \sqrt[3]{\frac{18}{\max(0,\sqrt{70}\cos(\sqrt{3}(x-t+5))+4)}}\\ &\quad\times \mathrm{e}^{\mathrm{i}(x-2t+W(t))}.\end{aligned} \tag{82}$$

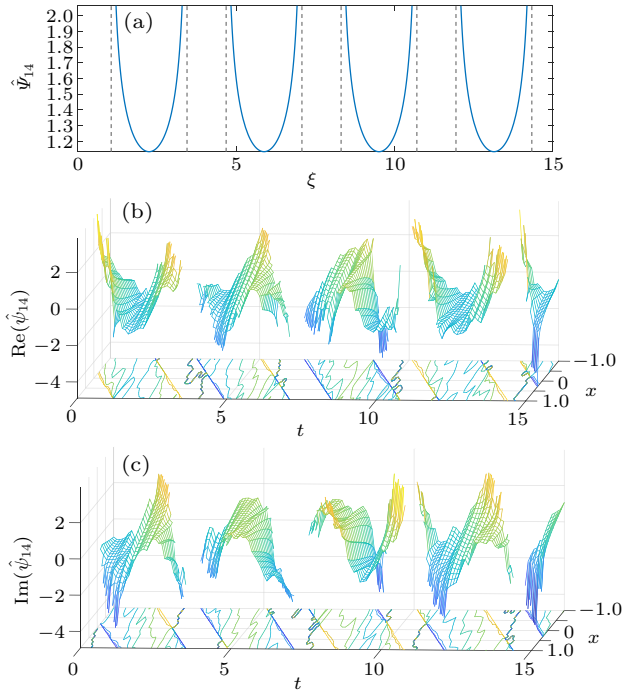


Fig. 13. Graphical illustration of $\hat{\Psi}_{14}$ and the specific solution $\hat{\psi}_{14}$ given in Eqs. (81) and (82), respectively. (a) The graph of the profile $\hat{\Psi}_{14}$. (b) The graph of $\mathrm{Re}(\hat{\psi}_{14})$. (c) The graph of $\mathrm{Im}(\hat{\psi}_{14})$.

Remark 3 As in Ref. [46], to plot the graphs of the specific exact solutions $\hat{\psi}_2(x,t)$, $\hat{\psi}_7(x,t)$, $\hat{\psi}_9(x,t)$ and $\hat{\psi}_{14}(x,t)$, given by Eqs. (76), (78), (80) and (82), respectively, i.e., Figs. 10–13, we simulated the Brownian motion $W(t)$, via adapting the classical Euler–Maruyama scheme[52] developed to solve numerically stochastic ODEs. Please see Ref. [46] for more details on the simulation of Brownian motion $W(t)$.

Remark 4 As revealed clearly in Figs. 10–13, the stochastic perturbation, described by multiplicative white noise based on Stratonvich's calculus, causes the graphs of the exact solutions to SSLSE (1) to wrinkle. As pointed in Refs. [45,46], we can infer that the larger the coefficient σ of the stochastic perturbation term $\sigma(\psi - \mathrm{i}c_3\psi_x)\circ\frac{\mathrm{d}W(t)}{\mathrm{d}t}$ is, the more wrinkled the graphs of the exact solutions of SSLSE (1) become.

6. Conclusion

In this paper, we studied the exact solutions to SSLSE (1) in which the calculus is taken in Stratonvich's sense. By mainly applying a series of changes of variables, we converted our primary problem of finding exact solutions (including soliton solutions) to SSLSE (1) into the task of finding exact solutions of a planar Hamiltonian dynamical system (see Eq. (19)). We studied the dynamical behaviors of planar Hamiltonian dynamical system (19). Aided by these obtained dynamics results, we computed exact solutions, of 14 forms and collected in Section 4, of SSLSE (1). In accordance with the exact solutions results presented in Section 4, we conducted several numerical simulations to validate the theoretical findings. As remarked in Ref. [2], SSLSE (1) can be used to model the propagation of pulses in optical fiber. Thus, our research lays the foundation for discovering new exact solutions optimized for optical communication and contributes to advancing optical technologies. As with Ref. [25], our model includes multiplicative white noise, which offers insights into both deterministic dynamics and random fluctuations within these complex systems.

Acknowledgements

Chengqiang Wang is partially supported by Qing Lan Project of Jiangsu, Suqian Sci. & Tech. Program (Grant Nos. Z2023131 and M202206), the Startup Foundation for Newly Recruited Employees, the Xichu Talents Foundation of Suqian University (Grant No. 2022XRC033), and the National Natural Science Foundation of China (Grant No. 11701050).

References

[1] Yang Y Q, Yan Z Y and Malomed B A 2015 *Chaos* **25** 103112
[2] Kudryashov N A 2021 *Mathematics* **9** 3024
[3] Ma W X, Osman M S, Arshed S, Raza N and Srivastava H M 2021 *Chin. J. Phys.* **72** 475
[4] Kudryashov N A 2020 *Optik* **206** 164335
[5] Wang T Y, Zhou Q and Liu W J 2022 *Chin. Phys. B* **31** 020501
[6] Zhang Y F, Wang H F and Bai N 2022 *Acta Math. Appl. Sin.* **38** 579
[7] Mirzazadeh M, Hashemi M S, Akbulu A, Rehman H U, Iqbal I and Eslami M 2024 *Math. Methods Appl. Sci.* **47** 5355
[8] Yildirim Y and Biswas A 2024 *Phys. Lett. A* **527** 129998
[9] Arnous A H, Murad M A S, Biswas A and Yildirim Y 2025 *Ain Shams Eng. J.* **16** 103243
[10] Zayed E M E, El-Shater M, Elsherbeny A M, Arnous A H, Biswas A, Yildirim Y, *et al.* 2025 *Ain Shams Eng. J.* **16** 103260
[11] Zhou Y Q, Liu Q, Zhang J and Zhang W N 2006 *Appl. Math. Comput.* **177** 495
[12] Zhou Y Q, Liu Q and Zhang W N 2011 *Nonlinear Anal.* **74** 1047
[13] Kumara S and Kumar A 2022 *Math. Comput. Simul.* **201** 254
[14] Li Y, Hao X Z, Yao R X, Xia Y R and Shen Y L 2023 *Math. Comput. Simul.* **208** 57
[15] Ashraf M A, Seadawy A R, Rizvi S T R and Althobaiti A 2024 *Opt. Quant. Electron.* **56** 1243
[16] Li Z and Liu C Y 2024 *Results Phys.* **56** 107305
[17] Zayed E M E, Nofal T A, Alngar M E M and El-Horbaty M M 2021 *Optik* **231** 166381
[18] Zhou Q, Huang Z H, Sun Y Z, Triki H, Liu W J and Biswas A 2022 *Nonlinear Dynam.* **111** 5757
[19] Zayed E M E, Gepreel K A and El-Horbaty M 2023 *Optik* **286** 170975
[20] Zayed E M E, Shohib R M A and Alngar M E M 2023 *Optik* **278** 170736
[21] Zayed E M E and Alngar M E M 2021 *Optik* **227** 166099
[22] Kudryashov N A 2022 *Optik* **259** 168975
[23] Secer A 2022 *Optik* **268** 169831
[24] Yildirim Y, Biswas A and Alshehri H M 2022 *Optik* **264** 169336
[25] Zayed E M E, Alngar M E M, Shohib R M A, Biswas A, Yildirim Y, Alshomrani A S and Alshehri H M 2022 *Optik* **264** 169369
[26] Zhou Q, Sun Y Z, Triki H, Zhong Y, Zeng Z L and Mirzazadeh M 2022 *Results Phys.* **41** 105898

[27] AlQahtani S A, Alngar M E M, Shohib R M A and Pathak P 2023 *Chaos Solitons Fract.* **171** 113498
[28] Chen D and Li Z 2023 *Optik* **277** 170687
[29] Cakicioglu H, Ozisik M, Secer A and Bayram M 2023 *Optik* **279** 170776
[30] Li R J, Sinnah Z A B, Shatouri Z M, Manafian J, Aghdaei M F and Kadi A 2023 *Results Phys.* **46** 106293
[31] Akram G, Sadaf M and Khan M A U 2023 *Math. Comput. Simul.* **206** 1
[32] El-Ganainia S and Kumarb S 2023 *Math. Comput. Simul.* **208** 28
[33] Izgi Z P 2023 *Math. Comput. Simul.* **208** 535
[34] Butt A R, Umair M and Basendwah G A 2024 *Optik* **308** 171801
[35] Lu T X, Tang L, Chen Y L and Chen C W 2024 *Results Phys.* **60** 107679
[36] Khan M I, Farooq A, Nisar K S and Shah N A 2024 *Results Phys.* **59** 107593
[37] Murad M A S, Ismael H F, Sulaiman T A and Bulut H 2024 *Opt. Quant. Electron.* **56** 76
[38] Trouba N T, Alngar M E M, Mahmoud H A and Shohib R M A 2024 *Ain Shams Eng. J.* **15** 103117
[39] Wazwaz A M 2024 *Ukr. J. Phys. Opt.* **25** S1131
[40] Liu L, Zhou X X, Xie X Y and Sun W R 2025 *Math. Comput. Simul.* **228** 466
[41] Yao Y L, Yi H H, Zhang X and Ma G L 2023 *Chin. Phys.. Lett.* **40** 100503
[42] Zhang X F, Xu T, Li M and Meng Y 2023 *Chin. Phys.. B* **32** 010505
[43] Yuan R R, Shi Y, Zhao S L and Wang W Z 2024 *Chaos Solitons Fract.* **181** 114709
[44] Zayed E M E, Alurrfi K A E, Hasek A M M, Arar N, Arnous A H and Yildirim Y 2024 *Phys. Scr.* **99** 095220
[45] Zayed E M E, Arnous A H, Secer A, Ozisik M, Bayram M, Shah N A and Chung J D 2024 *Results Phys.* **58** 107439
[46] Wang C Q, Zhao X Q, Mai Q Y and Lv Z W 2025 *Phys. Scr.* **100** 025257
[47] Chahlaoui Y, Shohib R M A and Alngar M E M 2024 *Opt. Quant. Electron.* **56** 1108
[48] Yi X Q, Zhou Y Q, Liu Q, Li K B and Zhang S N 2025 *Qual. Theory Dyn. Syst.* **24** 55
[49] Arshed S, Raza N and Alansari M 2021 *Ain Shams Eng. J.* **12** 3091
[50] Liu H D, Tian B, Gao X T, Shan H W and Ma J Y 2025 *Nonlinear Dyn.* **113** 12057
[51] Rehman H U, Aljohani A F, Althobaiti A, Althobaiti S and Iqbal I 2024 *Opt. Quantum Electron.* **56** 1336
[52] Kloeden P E and Platen E 1992 *Numerical Solution of Stochastic Differential Equations* (Heidelberg: Springer Berlin) pp. 305
[53] Al-Askar F M 2023 *Results Phys.* **52** 106784
[54] Fan E G 2002 *J. Phys. A Math. Gen.* **35** 6853
[55] Wazwaz A-M 2004 *Appl. Math. Comput.* **154** 713
[56] El-Wakil S A and Abdou M A 2007 *Chaos Solitons Fract.* **31** 840
[57] Wang M L, Li X Z and Zhang J L 2008 *Phys. Lett. A* **372** 417
[58] Zayed E M E and Gepreel K A 2009 *J. Math. Phys.* **50** 013502
[59] Liu C S 2010 *Comput. Phys. Commun.* **181** 317
[60] Li L X, Li E Q and Wang M L 2010 *Appl. Math. J. Chin. Univ.* **25** 454
[61] Srivastava H, Baleanu D, Machado J A T, Osman M S, Rezazadeh H, Arshed S and Günerhan H 2020 *Phys. Scr.* **95** 075217
[62] Tang L, Biswas A and Yildirim Y 2023 *Contemp. Math.* **4** 981
[63] Wang C Q, Zhao X Q, Mai Q Y and Lv Z W 2024 *Fractal Fract.* **8** 83
[64] Rahman M U, Sun M, Boulaaras S and Baleanu D 2024 *Bound. Value Probl.* **2024** 15
[65] Wang C Q, Zhao X Q, Zhang Y L and Lv Z W 2023 *Entropy* **25** 359
[66] Perko L 2001 *Differential Equations and Dynamical Systems* 3rd Edn. (New York: Springer) pp. 119–127
[67] Liu X M, Zhang Z Y and Liu W J 2023 *Chin. Phys. Lett.* **40** 070501